NACA TN 3695

NATIONAL ADVISORY COMMITTEE FOR AERONAUTICS

TECHNICAL NOTE 3695

AN ANALYSIS OF BUZZING IN SUPERSONIC RAM JETS BY A MODIFIED ONE-DIMENSIONAL NONSTATIONARY WAVE THEORY

By Robert L. Trimpi

Langley Aeronautical Laboratory
Langley Field, Va.

Washington
July 1956

NATIONAL ADVISORY COMMITTEE FOR AERONAUTICS

TECHNICAL NOTE 3695

AN ANALYSIS OF BUZZING IN SUPERSONIC RAM JETS BY A MODIFIED ONE-DIMENSIONAL NONSTATIONARY WAVE THEORY[1]

By Robert L. Trimpi

SUMMARY

Experimental instantaneous pressure records of simulated ram-jet models without heat addition showed that they "buzzed" in a manner governed internally by quasi-one-dimensional (plane-wave) theory and not in accord with the laws of the Helmholtz theory. A theory applicable to the buzzing problem was obtained by modification of the one-dimensional, unsteady-flow theory by introducing specified assumptions which greatly facilitated the computational efforts without impairing the usefulness of the theory for this flow. Because of the difficulty in computing the three-dimensional unsteady viscous flow when the shock was in motion ahead of the cowling and in computing when the shock was in motion far from equilibrium with the waves moving upstream from the nozzle, it was necessary to use a few experimental points at the start of the cycle as a basis on which to compute the many remaining pressure points of the cycle. Theoretical computations of the pressure-time curves, which were made on this basis for one supersonic-diffuser configuration with two different subsonic-duct lengths, agreed closely with the experimental records. The entrance and exit mass-flow—time curves, as well as the wave diagrams, were also computed for these configurations by the unsteady-flow theory. A possible simulation of the buzzing in ram jets with combustion by the test of a cold-flow model in which a contraction in area replaces the combustion chamber is also discussed.

INTRODUCTION

The buzz or pulsation of axially symmetric supersonic inlets having central bodies has been the subject of investigations since Oswatitsch first observed the phenomenon in 1944 (ref. 1). This buzzing is essentially an oscillation of the normal shock along the spike of certain

---

[1]Supersedes recently declassified NACA Research Memorandum L52A18 by Robert L. Trimpi, 1952.

diffusers operating at mass flows below design, and this buzz decreases the performance of the propulsion units appreciably (ref. 2). When a fixed-geometry ram jet is accelerated to the design Mach number, it is necessary to fly through a range of mass flows less than the design value. Consequently, the importance of either avoiding the conditions causing the buzz or reducing and controlling the amplitude of the oscillation is evident. In order to accomplish this end it is, of course, desirable to understand the complete nature of the phenomena. Antonio Ferri and Louis M. Nucci (ref. 3) have described one of the mechanisms which initiate the buzz. This paper continues the analysis of the buzzing cycle by means of a modified one-dimensional approach. The buzzing referred to herein is not to be confused with the pulsations of inlets sometimes observed due to improper operation of the combustion system.

The causes of this buzz, in the absence of combustion, have been studied previously and include effects due to the presence of separation inside the entrance to the cowling. The choking resulting from this separation reduces the internal mass flow and forces the normal shock to move forward; thus, the buzz is initiated. Reference 3 has shown that this separation is often due to a vortex sheet near the inner wall of the cowling lip. This vortex sheet arises from the intersection of either the conical and normal shocks or, in some cases of separation on the central body giving rise to lambda shocks, from the intersection of the legs of the lambda shock. In certain instances, the separated flow from the central body has appeared sufficient in itself to choke the cowling and precipitate the pulsations. As the buzzing cycle progresses, the normal shock moves rearward and assumes a position where it may remain for an appreciable time, depending on internal-flow considerations, before the start of the next oscillation.

Some very general theories based on internal mass-flow considerations have been expounded which give little insight into the aerodynamic nature of the phenomena making up the complete buzz cycle (refs. 3 and 4). An attempt has also been made (ref. 5) to predict the frequency only of the buzz by considering a ram jet to be similar to a Helmholtz resonator. The application of a quasi-one-dimensional theory to the buzz problem would seem proper from considerations of the ram-jet geometry. First of all, the area variations are gradual because of the necessity for high diffuser performance. Furthermore, the ratio of maximum area of the unit to the minimum area usually varies from 3 to 5; whereas for the passages of the internal-flow system the ratio of the length to the maximum diameter is generally in the range of 6 to 15. These proportions suggest the use of an unsteady-flow theory, such as a quasi-one-dimensional one, which assumes a slight variation of the moving pressure waves from the plane form, rather than a Helmholtz type theory based on two- or three-dimensional waves (that is, large, abrupt area changes).

Consequently, an appropriate modified one-dimensional nonstationary-flow wave theory has been derived at the Langley laboratory. This theory assumes quasi-steady flow for the reflections of upstream-moving waves which strike the normal shock and for waves passing through an area change. Because of the difficulty in computing the three-dimensional, nonsteady phenomenon which occurs as the normal shock moves rapidly outward and inward during part of the cycle, it is necessary to use a few experimentally determined values of the waves generated by this motion as a basis on which to compute the remainder of the cycle. For the particular cycles computed in this paper, four or five experimentally determined instantaneous pressures are used to compute one hundred or more additional pressure points required to complete the cycle. Once the initial problem has been specified by the experimental points, however, the remainder of the solution is easily obtained from graphs with a minimum of computation and good degree of precision.

SYMBOLS

a	local speed of sound
A	area measured normal to ram-jet axis
C_I, C_{II}	characteristic parameters for steady flow
C_p	coefficient of specific heat at constant pressure
C_v	coefficient of specific heat at constant volume
h	state ahead of typical downstream wave
j	state behind a typical downstream wave
k	state behind reflection from a typical downstream wave
L	distance from cowling inlet to exit nozzle of ram jet
m	mass flow
m_∞	mass flow at infinity through a stream tube of diameter equal to cowling lip diameter
M	Mach number
p	local static pressure

$$P = \frac{2}{\gamma - 1}\frac{a}{a_{O_\infty}} + \frac{u}{a_{O_\infty}}$$

$$Q = \frac{2}{\gamma - 1}\frac{a}{a_{O_\infty}} - \frac{u}{a_{O_\infty}}$$

} characteristic parameters for unsteady flow

P_3' characteristic parameter reflected at cowling by parameter Q_3 for case when both parameters are evaluated in fluid having entropy equal to "effective value"

R gas constant

S/R nondimensional entropy referred to free-stream datum

t time, sec

T local static temperature

ΔT_O energy added to flow across flame front

u local fluid speed

x coordinate along ram-jet axis

γ ratio of specific heats, assumed equal to 1.400

ϵ distance from flame front or area contraction to exit nozzle

θ_l angle included between ram-jet axis and line from apex of spike to cowling lip

ρ local static density

Subscripts:

b state in ram jet at start of buzz

c,d states on opposite side of typical entropy discontinuity

e effective one-dimensional values

f,g states on opposite side of entropy discontinuity entering exit nozzle

i station at cowling inlet (total cross section enclosed by inlet)

n	exit nozzle (measured, not effective, value)
q	state behind an upstream wave generated by entropy discontinuity passing through nozzle
r	state behind second entropy discontinuity entering exit nozzle
∞	free-stream state
α	region between flame front and nozzle of ram jet
β	region between area contraction and nozzle of ram jet
o	state obtained by isentropic deceleration from static conditions to zero velocity
1	annular station at cowling inlet
2	station immediately behind cowling in a simplified ram jet
3	station immediately ahead of nozzle in a simplified ram jet

Except for the cases noted in symbol list, subscripts denote the evaluation at the state or station designated by the subscript. A bar over a symbol indicates an average over a cycle.

THEORY

Basic Theory

One-dimensional unsteady-flow characteristic theory is governed by the following differential equations, which determine the variation of the parameters P and Q, respectively, along the corresponding characteristic lines having slopes of $\frac{dx}{dt} = u + a$ and $\frac{dx}{dt} = u - a$

$$\frac{\delta P}{\delta t} = -\frac{a}{a_{o_\infty}} \frac{D \log_e A}{Dt} + \frac{\gamma - 1}{\gamma} \frac{a}{a_{o_\infty}} \frac{D \frac{S}{R}}{Dt} + \frac{1}{\gamma} \frac{a}{a_{o_\infty}} \frac{\delta \frac{S}{R}}{\delta t} \tag{1}$$

$$\frac{\delta Q}{\delta t} = -\frac{a}{a_{o_\infty}} \frac{D \log_e A}{Dt} + \frac{\gamma - 1}{\gamma} \frac{a}{a_{o_\infty}} \frac{D \frac{S}{R}}{Dt} + \frac{1}{\gamma} \frac{a}{a_{o_\infty}} \frac{\delta \frac{S}{R}}{\delta t} \tag{2}$$

$$P \equiv \frac{2}{\gamma - 1}\frac{a}{a_{O_\infty}} + \frac{u}{a_{O_\infty}} \tag{3}$$

$$Q \equiv \frac{2}{\gamma - 1}\frac{a}{a_{O_\infty}} - \frac{u}{a_{O_\infty}} \tag{4}$$

where $\frac{\delta(\ )}{\delta t} = \frac{\partial(\ )}{\partial t} + (u \pm a)\frac{\partial(\ )}{\partial x}$ is the total variation along a characteristic and $\frac{D(\ )}{Dt} = \frac{\partial(\ )}{\partial t} + u\frac{\partial(\ )}{\partial x}$ is the variation of a particular fluid particle.

These equations are derived in appendix A by combination of the equations of energy, momentum, continuity, and state. Equations of similar type may be found in reference 6 in which, however, the area is not considered to be time dependent.

The parameters P and Q have much the same relation to unsteady-flow theory as the parameters C_I and C_{II} have to the Prandtl-Busemann characteristic theory for steady flow (for example, see reference 7). In the two-dimensional steady-flow system, C_I and C_{II} are invariant along characteristic lines of the first and second family except when the characteristics pass through rotational flow fields. The parameters C_I and C_{II} may vary in an irrotational three-dimensional flow because of the effects of stream-tube-area change. Similarly, in one-dimensional unsteady flow, the values of P and Q are constant along the characteristics except when influenced by entropy changes or area changes (the latter factor influences the parameters by accounting for the variation of the flow from the exact one-dimensional flow). In steady flow the inclination of the streamlines is proportional to the differences of C_I and C_{II} whereas the velocity is proportional to their sum. Again there is a similarity in one-dimensional unsteady flow where the particle speed is proportional to the difference of P and Q whereas the local speed of sound is proportional to their sum.

In the use of the one-dimensional characteristic equations above, a very lengthy and tedious step-by-step process is required to obtain a solution. Consequently, certain simplifications and assumptions are made to obtain a modified theory which appreciably facilitates the procedure necessary to obtain a solution.

Modified Theory

In the interest of simplicity and computational facilities, the basic theory has been modified by application of the following assumptions.

Substitution of discontinuous area changes for area gradients.- In order to simplify the solution, gradual variations in cross section are accumulated and treated as discontinuous area changes. Thus, the actual ram jet, as shown in figure 1(a), is assumed to have the shape of figure 1(b) where the only area changes appear at the cowling and the nozzle exit. The penalty for a considerable reduction in computation is a time distortion in the wave pattern since both the duration and time of generation of reflections is greatly reduced. In other words, the unmodified solution yields gradual reflections as soon as an area gradient is encountered by a wave. No reflections, however, can arise in the simplified ram jet until a wave hits either end of the duct, whereupon stronger reflections, representing the accumulation of the aforementioned gradual reflections, are generated.

Restriction requiring equality of entropy of a fluid particle at both entrance and exit of hypothetical ram jet.- In order to simplify the procedure further, all waves moving through the duct proper are assumed to be isentropic. Thus, the entropy increase in the fluid is assumed to be the cumulative result of the conical shock, normal shock, and separation on the central body preceding the main duct. The entropy of entering fluid particles varies only as these factors vary and then this entropy (which may have a different value for various particles) remains constant for a particular fluid particle flowing along the duct.

Use of quasi-steady flow to obtain reflections at duct exit and entrance.- The assumption of quasi-steady flow is introduced to provide a simple solution for the integrated form of the characteristic equations when waves pass through area changes or encounter the normal shock. This modification is based on the fact that steady flow is established at an area change in a very short time interval after the passage of the initial wave. Consequently, all the minor transmitted and reflected waves may be accumulated with the major transmitted and reflected waves, and then the group treated as consisting of only one transmitted and one reflected wave. Of course, this treatment also yields a wave pattern with a slight time distortion, but, in view of the labor saved, this distortion is justifiable.

The reflection condition at the nozzle exit is then easily determined. Since the subsequent analysis is to be limited to supersonic flight for which the pressure in the duct is always greater than the stagnation pressure required to produce sonic velocity by isentropic expansion to atmospheric pressure, the boundary condition of sonic velocity in the nozzle is dictated. Consequently, since the ratio of

the area of the duct to the nozzle area is invariant, there is automatically imposed the condition of constant Mach number (which must be equal to the effective Mach number at the start of buzz) in the ram jet just ahead of the nozzle under the assumption of quasi-steady flow. Thus, from the definitions of P and Q, one finds for the values of these parameters existing just ahead of the nozzle

$$M_e = \frac{u_e}{a_e} = \frac{\frac{P_3 - Q_3}{2}}{\frac{P_3 + Q_3}{\frac{4}{\gamma - 1}}} \tag{5}$$

or

$$\frac{Q_3}{P_3} = \frac{\frac{2}{\gamma - 1} - M_e}{\frac{2}{\gamma - 1} + M_e} = \frac{5 - M_e}{5 + M_e} \quad \text{for} \quad \gamma = 1.400 \tag{6}$$

where M_e is the effective Mach number of the duct. Thus, the value of the parameter P_3 for a characteristic moving downstream at the nozzle uniquely specifies the parameter Q_3 of the reflected-upstream characteristic.

For the case of reflections from the cowling inlet of upstream-traveling waves, the parameter P can be evaluated if the mass flow entering the cowling is known. During a large part of some cycles the normal shock is inside the cowling and therefore the mass flow may be determined from conical-flow theory and the external geometry. For that part of certain other cycles when the normal shock is ahead of the cowling but has not progressed out as far as the point where buzz starts, experimental steady-flow values of the mass flow can be used. Once the value of the mass flow is assumed, then there exists a relation at the cowling entrance between P, Q, the entropy S/R, and the effective area A_e for quasi-steady flow. As an illustration, assume that the external geometry is such that the conical shock intersects the cowling lip (that is, diffuser operating at design M_∞) while the normal shock is swallowed. Then the following equations of continuity, energy, and so forth, apply for quasi-steady flow:

$$A_i \rho_\infty M_\infty a_\infty = A_e \rho_2 M_2 a_2 \tag{7}$$

$$a_{o_\infty} = a_{o_2} \tag{8a}$$

$$\frac{\gamma - 1}{2}\left(\frac{u_\infty}{a_{o_\infty}}\right)^2 + \left(\frac{a_\infty}{a_{o_\infty}}\right)^2 = \frac{\gamma - 1}{2}\left(\frac{u_2}{a_{o_\infty}}\right)^2 + \left(\frac{a_2}{a_{o_\infty}}\right)^2 = 1.0 \tag{8b}$$

Introduction of the entropy term into equation (7) leads to

$$\frac{M_2}{M_\infty}\left(\frac{a_2}{a_\infty}\right)^{\frac{\gamma+1}{\gamma-1}} = \frac{A_i}{A_e}\, e^{\frac{S_2 - S_\infty}{R}} \tag{9}$$

In terms of P and Q equations (8b) and (9) become

$$\frac{\gamma - 1}{2}\left(\frac{P_2 - Q_2}{2}\right)^2 + \left(\frac{\gamma - 1}{4}\right)^2 (P_2 + Q_2)^2 = 1 \tag{10}$$

$$\left(\frac{P_2 - Q_2}{2}\right)\left[(P_2 + Q_2)\frac{\gamma - 1}{4}\right]^{\frac{2}{\gamma-1}} = \left(\frac{a_\infty}{a_{o_\infty}}\right)^{\frac{\gamma+1}{\gamma-1}} M_\infty \frac{A_i}{A_e}\, e^{\frac{S_2 - S_\infty}{R}} \tag{11}$$

Equations (10) and (11), plus the restriction that $u > 0$, which requires $P > Q$, uniquely determine the value of P for a given Q and S/R, or vice versa.

Before the reflected P_3' can be determined, however, the value of Q_2 must be found from the corresponding value of Q_3 along the same upstream characteristic (fig. 2). This value of Q_2 may be obtained from equation (2) which states, for A = constant and for isentropic flow of each elemental fluid volume $\left(\frac{D\frac{S}{R}}{Dt} = 0\right)$,

$$Q_3 - Q_2 = \int_2^3 \frac{1}{\gamma}\frac{a}{a_{o_\infty}}\, d\frac{S}{R} = \frac{1}{\gamma}\sum \frac{a}{a_{o_\infty}}\frac{\Delta S}{R} \tag{12}$$

For the low Mach numbers encountered in a ram-jet diffuser $\frac{a}{a_{0_\infty}} \approx 1$, equation (12) becomes

$$Q_3 - Q_2 \doteq \frac{1}{\gamma} \frac{\bar{a}}{a_{0_\infty}} \sum \frac{\Delta S}{R} \doteq \frac{1}{\gamma} \frac{S_3 - S_2}{R} \tag{13}$$

Similarly,

$$P_3 - P_2 \doteq \frac{1}{\gamma} \frac{S_3 - S_2}{R} \tag{14}$$

Therefore, since $\frac{S_3}{R}$ is known from the starting conditions and, for a given value of $\frac{S_2}{R}$, P_2 and Q_2 are specified, one can determine from equations (10), (11), (13), and (14) the value of the reflected characteristic parameter P_3'. The detailed procedure to find P_3' for a specific Q_3 would be the following (see fig. 2):

(1) Equation (10) is solved for P_2 in terms of Q_2.

(2) This value of P_2 is substituted into equation (11) so that it becomes an equation of the form: $Q_2 = Q_2\left(\frac{S_2}{R}\right)$.

(3) This equation for Q_2 is then plotted together with equation (13), which is also in the form $Q_2 = Q_2\left(\frac{S_2}{R}\right)$, and the intersection of the two curves determines the correct value of S_2/R and Q_2.

(4) The value of P_2 is then found from Q_2 and equation (10).

(5) The term P_3' is then evaluated by equation (14).

The most convenient method of obtaining the values of P_3' from Q_3, however, has been found to use a plot of P_3' against Q_3 where P_3' and Q_3 are computed by adjusting each point of the curve for $P_2\left(\frac{S_2}{R}\right)$ against $Q_2\left(\frac{S_2}{R}\right)$ of equations (10) and (11) by a factor of $\frac{1}{\gamma} \frac{S_3 - S_2}{R}$.

This manner of determining the reflection at the forward section of the ram jet is inapplicable when the motion of the normal shock is far from a quasi-steady, or near equilibrium, state with the waves which have come upstream from the nozzle. In other words, when the shock has been set in motion from a point on the external spike owing to three-dimensional waves emanating from the cowling and then the shock enters the cowling, it may not be in equilibrium with the one-dimensional waves existing inside. Another case where the method is inapplicable would be the time when separation generated at the foot of the shock causes the shock to move, regardless of the upstream waves from the throat.

In addition, the use of some three-dimensional unsteady-flow characteristic theory in the presence of viscosity would be necessary to determine the reflection pattern from the normal shock when it is in motion ahead of the cowling. For these reasons, experimental pressures are used to prescribe the downstream waves generated when the normal shock is in motion either ahead of the cowling or else too rapidly for quasi-steady flow. In the cycles computed in this paper, both conditions occur simultaneously and necessitate the specification of only a few waves.

Reference of characteristic parameters to the basic entropy and subsequent neglect in wave diagram of entropy discontinuities in duct.- Although the variation with time of the entropy of the fluid entering the duct is allowed, the sweeping modification is employed of referring all the characteristic parameters to the basic effective entropy (that is, effective entropy of the fluid present in the duct at start of buzz). This assumption drastically reduces the computational effort, since it eliminates the determination of an entropy-discontinuity streamline every time a wave strikes the normal shock and, then in turn, the determination of reflected and transmitted waves each time a wave impinges on these entropy discontinuities. It is also consistent with the assumption that $\frac{a}{a_{O_\infty}} \approx 1$ in equations (13) and (14) relating the increment of P or Q to the entropy variation across a discontinuity, since that assumption also implies the neglect of waves reflected from such discontinuities.

The use of a basic entropy simply amounts to the insertion of an imaginary lamina of fluid having the "basic entropy" in a fluid of another value of entropy in order to determine the pressure and velocity, but not the density, of the flow. This procedure is permissible because the last terms in equations (1) and (2) represent the increment in the characteristic parameters P and Q across an entropy discontinuity when the pressure and velocity are constant. This fact may be proven as follows with reference to figure 3. By applying the definitions of P and Q to the characteristics in figure 3, the following equations are determined:

$$P_d - P_c = \frac{2}{\gamma - 1}\frac{a_d}{a_{o_\infty}} + \frac{u_d}{a_{o_\infty}} - \left(\frac{2}{\gamma - 1}\frac{a_c}{a_{o_\infty}} + \frac{u_c}{a_{o_\infty}}\right) = \frac{2}{\gamma - 1}\frac{(a_d - a_c)}{a_{o_\infty}} \tag{15}$$

$$Q_d - Q_c = \frac{2}{\gamma - 1}\frac{a_d}{a_{o_\infty}} - \frac{u_d}{a_{o_\infty}} - \left(\frac{2}{\gamma - 1}\frac{a_c}{a_{o_\infty}} - \frac{u_c}{a_{o_\infty}}\right) = \frac{2}{\gamma - 1}\frac{(a_d - a_c)}{a_{o_\infty}} \tag{16}$$

since $u_c = u_d$.

Therefore,

$$\Delta P = \Delta Q = \frac{2}{\gamma - 1}\frac{(a_d - a_c)}{a_{o_\infty}} = \frac{2}{\gamma - 1}\frac{a_c}{a_{o_\infty}}\left(\frac{a_d}{a_c} - 1\right) \tag{17}$$

Introduction of entropy into equation (17) yields

$$\Delta P = \Delta Q = \frac{2}{\gamma - 1}\frac{a_c}{a_{o_\infty}}\left[e^{\frac{\gamma-1}{2\gamma}\frac{\Delta S}{R}}\left(\frac{p_d}{p_c}\right)^{\frac{\gamma-1}{2\gamma}} - 1\right] \tag{18}$$

$$= \frac{2}{\gamma - 1}\frac{a_c}{a_{o_\infty}}\left[\frac{\gamma - 1}{2\gamma}\frac{\Delta S}{R} + \frac{1}{2}\left(\frac{\gamma - 1}{2\gamma}\frac{\Delta S}{R}\right)^2 + \cdots\right] \text{ since } p_d = p_c \tag{19}$$

$$\approx \frac{1}{\gamma}\frac{\Delta S}{R} \quad \text{for} \quad \frac{a_c}{a_o} \approx 1, \quad \frac{\Delta S}{R} \ll 1 \tag{20}$$

Now, in figure 3(b) the true values of Q and P in the fluid of entropy $\frac{S_d}{R}$ were determined as specified by equations (13) and (14) from the corresponding values in the fluid of entropy $\frac{S_3}{R}$ by adding the correction $\frac{1}{\gamma}\frac{S_d - S_3}{R}$. Consequently, when they are reduced to the basic entropy $\frac{S_3}{R}$ of the imaginary lamina inserted in the fluid, the

factor $\frac{1}{\gamma}\frac{S_3 - S_d}{R}$ $\left(\text{that is, } \frac{1}{\gamma}\frac{\Delta S}{R} \text{ from equation (20)}\right)$ must be added, and the original values of P_3 and Q_3 are recovered.

The relationship between the pressure and sonic speed within a fluid of constant entropy is:

$$\frac{p}{p_e} = \left(\frac{a}{a_e}\right)^{\frac{2\gamma}{\gamma-1}} = \left(\frac{P + Q}{P_e + Q_e}\right)^{\frac{2\gamma}{\gamma-1}} \tag{21}$$

Since the pressure and velocity, but not density, are invariant across an entropy discontinuity in the flow, it is permissible to ignore the variation in entropy and use the values of P and Q based on the effective entropy $\frac{S_3}{R}$ at the start of buzz for the computation of pressure as $\frac{p}{p_e} = \left(\frac{P + Q}{P_e + Q_e}\right)^{\frac{2\gamma}{\gamma-1}}$ and velocity as $\frac{u}{a_{o_\infty}} = \frac{P - Q}{2}$ in any part of the fluid regardless of entropy. The wave diagram will then be greatly simplified, but will not be a true picture of the flow in regard to stream density or mass flow.

Of course, if the entropy at a point is known, the mass flow can be determined from the values of P and Q in the imaginary lamina of basic entropy. When reference is made to figure 3(b) where conditions c correspond to the imaginary lamina,

$$\frac{m_c}{m_d} = \frac{\rho_c u_c}{\rho_d u_d} \tag{22}$$

$$= \left(\frac{p_c}{p_d}\right)^{\frac{1}{\gamma}} e^{\frac{\gamma-1}{\gamma}\frac{S_d - S_c}{R}} \frac{u_c}{u_d} \tag{23}$$

$$= e^{\frac{S_d - S_c}{R}\frac{\gamma-1}{\gamma}} \quad \text{since } p_c = p_d, \; u_c = u_d \tag{24}$$

When equation (24) is expanded and higher order terms are neglected,

$$\frac{m_d}{m_c} = e^{\frac{S_c - S_d}{R}\frac{\gamma-1}{\gamma}} \approx 1 + \frac{\gamma - 1}{\gamma}\frac{S_c - S_d}{R} + \cdots \tag{25}$$

The ratio of

$$\frac{m_c}{m_b} = \left(\frac{\rho_c}{\rho_b}\right)\left(\frac{u_c}{u_b}\right) = \left(\frac{a_c}{a_b}\right)^{\frac{2}{\gamma-1}}\left(\frac{u_c}{u_b}\right) \tag{26}$$

since

$$\frac{S_c}{R} = \frac{S_b}{R} = \frac{S_e}{R} \tag{27}$$

Then equation (26) becomes

$$\frac{m_c}{m_b} = \left(\frac{P_c + Q_c}{P_b + Q_b}\right)^{\frac{2}{\gamma-1}}\left(\frac{P_c - Q_c}{P_b - Q_b}\right) \tag{28}$$

Thus the ratio of the actual mass flow to the mass flow at the start of buzz becomes.

$$\frac{m_d}{m_b} = \frac{m_d}{m_c}\frac{m_c}{m_b} = \left(\frac{P_c + Q_c}{P_b + Q_b}\right)^{\frac{2}{\gamma-1}}\left(\frac{P_c - Q_c}{P_b - Q_b}\right)\left(1 + \frac{\gamma - 1}{\gamma}\frac{S_e - S_d}{R}\right) \tag{29}$$

There still remains the problem of determining the local entropy. This task, if it is to be precisely accomplished, requires the plotting of the entropy-discontinuity space-time histories. Without these histories, however, it is possible to obtain easily a so-called "extrapolated value" of the mass flow entering the cowling by assuming quasi-steady flow from infinity to the cowling lip. This value is not a true value when the

shock is inside the cowling and out of equilibrium with the upstream Q waves, since the mass flow entering must be equal to m_∞ when the conical shock is at the lip of the cowling. This error is due to the fact that the parameters P and Q were determined experimentally at stations to the rear of the shock and included the effect of the shock motion. Consequently, use of these P and Q terms evaluated at $\frac{x}{L} = 0$ give the mass flow just behind the shock instead of at the cowling entrance so that the values are only correct when the shock is ahead of the cowling or when it is in equilibrium inside the cowling. Since these parameters determine the local pressure and velocity, the assumption of quasi-steady flow permits the determination of the local temperature from the energy equation. Then, when the pressure and the temperature are known, the local entropy and, in turn, the mass flow may be found.

When the presence of entropy discontinuities in the flow is disregarded in the wave diagram, the waves originating from the arrival of these discontinuities at changes in cross section are, of course, omitted. In particular, the upstream wave generated by the passage of a discontinuity through the choked exit nozzle is neglected and this omission must be justified. Figure 4 shows the wave pattern in the diffuser created by the passage of an entropy change through the nozzle. The following relations then apply

$$Q_f = \frac{\frac{2}{\gamma - 1} - M_e}{\frac{2}{\gamma - 1} + M_e} P_f \tag{30}$$

$$Q_g = Q_f + \frac{\Delta S}{\gamma R} \quad \text{where} \quad \frac{\Delta S}{R} = \frac{S_g - S_f}{R} \tag{31}$$

$$P_g = P_f + \frac{\Delta S}{\gamma R} \tag{32}$$

$$Q_q = \frac{\frac{2}{\gamma - 1} - M_e}{\frac{2}{\gamma - 1} + M_e} P_g = \frac{\frac{2}{\gamma - 1} - M_e}{\frac{2}{\gamma - 1} + M_e}\left(P_f + \frac{\Delta S}{\gamma R}\right) - \tag{33}$$

$$= Q_f + \frac{\frac{2}{\gamma - 1} - M_e}{\frac{2}{\gamma - 1} + M_e} \frac{\Delta S}{\gamma R} \tag{34}$$

$$= Q_g + \frac{\Delta S}{\gamma R}\left(\frac{\frac{2}{\gamma - 1} - M_e}{\frac{2}{\gamma - 1} + M_e} - 1\right) \tag{35}$$

$$Q_q - Q_g = -\frac{2M_e}{\frac{2}{\gamma - 1} + M_e} \frac{S_g - S_f}{\gamma R} \tag{36}$$

Thus, waves of strength $Q_q - Q_g$ are omitted in a solution neglecting entropy discontinuities (which is equivalent to the assumption $M_e \frac{(S_g - S_f)}{R} \ll 1$). In cases where this assumption is not justified, but another entropy discontinuity $\frac{S_r - S_g}{R}$ having opposite sign so that $\frac{S_r}{R} - \frac{S_f}{R} \ll 1$ soon follows the initial discontinuity through the area change, then the assumption has only introduced a time distortion in the wave pattern by treating a positive wave followed by an approximately equal negative wave as a single wave of zero strength.

Effective values employed in the modified theory.- One-dimensional flow presumes no variation of the flow properties in a direction normal to the stream velocity. Consequently, in order to apply such a theory to an actual ram jet where boundary-layer separation and centrifugal force actually cause a variation in the fluid properties across a section of the flow, effective values of the fluid properties and cross-sectional area must be employed. The effective values are defined as

the values satisfying the one-dimensional channel-flow relationships regarding continuity, energy, momentum, and the equation of state.

Since the effective area and Mach number A_e and M_e have such an important role in the theory, the equations which determine them are presented. Steady flow is assumed to exist for an infinitesimal time before buzz is started.

The mass flow at start of buzz is

$$m_b = \rho_e M_e a_e A_e = \rho_\infty M_\infty a_\infty A_i \frac{m_b}{m_\infty} \tag{37}$$

and

$$M_e = M_\infty \frac{a_\infty}{a_e} \frac{\rho_\infty}{\rho_e} \frac{A_i}{A_e} \frac{m_b}{m_\infty} \tag{38}$$

From the definition of entropy and equation of state,

$$\frac{\rho_\infty}{\rho_e} = \left(\frac{a_\infty}{a_e}\right)^{\frac{2}{\gamma-1}} e^{\frac{S_e - S_\infty}{R}} \tag{39}$$

Since $a_{o_\infty} = a_{o_e}$ at start of buzz, equation (39) becomes

$$\frac{\rho_\infty}{\rho_e} = \left(\frac{a_\infty}{a_e}\right)^{\frac{2}{\gamma-1}} \left(\frac{p_{o_\infty}}{p_{o_e}}\right)_b \tag{40}$$

Combining equations (38) and (40) yields

$$M_e = M_\infty \left(\frac{a_\infty}{a_e}\right)^{\frac{\gamma+1}{\gamma-1}} \left(\frac{p_{o_\infty}}{p_{o_e}}\right)_b \frac{A_i}{A_e} \left(\frac{m_b}{m_\infty}\right) \tag{41}$$

Insertion of energy equation into equation (41) gives

$$M_e = M_\infty \frac{\left(1 + \frac{\gamma - 1}{2} M_e^2\right)^{\frac{\gamma+1}{2(\gamma-1)}}}{\left(1 + \frac{\gamma - 1}{2} M_\infty^2\right)^{\frac{\gamma+1}{2(\gamma-1)}}} \left(\frac{p_{o_\infty}}{p_e}\right)_b \left(\frac{p_e}{p_{o_e}}\right)_b \frac{A_i}{A_e} \left(\frac{m_b}{m_\infty}\right) \tag{42}$$

$$M_e \left(1 + \frac{\gamma - 1}{2} M_e^2\right)^{\frac{1}{2}} = M_\infty \left(\frac{p_{o_\infty}}{p_e}\right)_b \left(\frac{A_i}{A_e}\right) \left(\frac{m_b}{m_\infty}\right) \left(1 + \frac{\gamma - 1}{2} M_\infty^2\right)^{-\frac{\gamma+1}{2(\gamma-1)}} \tag{43}$$

The specification of A_e plus experimental values for the other terms on the right-hand side of equation (43) prescribes M_e uniquely.

Approximation for simplifying construction of characteristic diagram.- Instead of the step-by-step procedure of constructing the characteristic lines with local slopes dependent on the sum or difference of the local fluid speed and sonic speed, the value of these speeds at the ends of the duct is used to obtain an average slope. Thus characteristic lines of the first family are drawn with a slope

$$\frac{d\frac{x}{L}}{dt} = \frac{\frac{u}{a_{o_\infty}} + \frac{a}{a_{o_\infty}}}{\frac{L}{a_{o_\infty}}} \tag{44}$$

evaluated as the average of the velocities for $\frac{x}{L} = 0$ and $\frac{x}{L} = 1$. Similarly, for the second family,

$$\frac{d\frac{x}{L}}{dt} = \frac{\frac{u}{a_{o_\infty}} - \frac{a}{a_{o_\infty}}}{\frac{L}{a_{o_\infty}}} \tag{45}$$

whereas for particle space-time histories

$$\frac{d\frac{x}{L}}{dt} = \frac{\frac{u}{a_{O_\infty}}}{\frac{L}{a_{O_\infty}}} \tag{46}$$

A linear variation of the parameters is used for interpolation between characteristics of the same family.

The characteristic theory has been greatly simplified so that the solution is easily obtained with the help of three plots, namely, (a) pressure-sonic velocity, $p = p_e\left(\frac{a}{a_e}\right)^{\frac{2}{\gamma-1}}$, (b) P - Q reflections at cowling inlet, and (c) Q - P reflections at the sonic nozzle. (See, for example, appendix B and figs. 25 and 26 for typical solutions using these plots.) After the experimental values of the few waves generated by the external motion of the normal shock are plotted, the remainder of the solution consists of reading values off the curves and plotting the characteristics.

APPARATUS

The apparatus employed for the experiments is shown in figure 5 and is essentially the same as that used in reference 3 with certain modifications necessary for the conversion from steady-flow to unsteady-flow measurements. The total-pressure rake at the survey plane ($x = 11.50$ inches), figure 5, was removed and an instantaneous static-pressure pickup employed in its place. The instantaneous pressure pickups were NACA miniature electrical pressure gages mounted flush with the diffuser wall. Also, since only reflections from the nozzle exit were desired, the mass-flow orifice was eliminated.

Tests were made at a Mach number of 1.9 in the Langley 4-inch by 5-inch blowdown open jet by using low-humidity air from pressurized tanks. The test Reynolds number based on cowling-inlet diameter was in the range between 2.9×10^6 and 3.6×10^6. Three different subsonic-duct lengths of 34 inches, 156 inches, and 390 inches were employed with instantaneous pressure pickups located along the diffuser as shown schematically in figure 6. The 90° elbows necessary to attain the desired duct lengths within the space limitations of the laboratory are indicated. The length of the central bodies (which had the same after-section in all cases) relative to diffuser lengths is also shown.

Tests were made on the three supersonic-diffuser configurations listed in the table below:

Configuration	Semicone angle (deg)	Maximum diameter of central body (in.)	Cowling (reference 3)	Values of cowling-position parameters (θ_l)
I	25	0.80	E	44° 0', 40° 40', 36° 50'
II	25	1.10	D	43° 10', 39° 50', 36° 50'
III	30	0.80	E	48° 30', 43° 40', 40° 40'

The dimensions of these central bodies and cowlings are given in reference 3 with the exception of the central body of configuration I, the dimensions of which are given in figure 7.

A commercial concentrated arc light served as the source for a shadowgraph system in which the image on a ground-glass screen was recorded on either of two 16-millimeter motion-picture cameras. For the longer diffuser lengths a low-speed camera operating at 64 frames per second was used, whereas for the short diffuser a Wollensak Optical Company Fastax camera running approximately 500 frames per second was employed. Signals from the pressure gages were amplified by a Consolidated type 1-113 amplifier and then recorded on sensitized paper in a Consolidated type 5-114 recorder employing galvanometer elements. The frequency response of this system was flat from 2 to 300 cycles per second. In order to correlate movie film with the pressure records, a timing light was attached to one edge of the shadowgraph glass screen and the circuit energizing this light connected in parallel with one of the recording galvanometers so that every time the light flashed a "blip" appeared on the pressure record. A synchronizing device was attached to the low-speed camera which flashed the light on the shadowgraph screen once each frame, while 60-cycle alternating current was used to operate the light when the Fastax camera was used. In order to reduce the labor of correlation, an interrupter was placed in the light circuit to stop the flow of current for a noticeable period four or five times a second, and hence provide blank spaces on the film and pressure record which could be easily counted.

A manually operated, 2-inch gate valve served as the exit throttle. Throttle position was recorded on the pressure film by means of an electrical circuit employing a ten-turn linear potentiometer attached to an extension of the valve stem.

TEST PROCEDURE

Tests of the various configurations were made by the following procedure: the desired central-body projection was set by scale measurement and, with no tunnel air flowing, a trace was then recorded on the pressure film; in the cases of runs made with the 64-frames-per-second motion-picture camera, a strip of "no flow" motion-picture film was also made. The exit throttle was opened to such an extent that the mass flow would be limited only by the supersonic-diffuser configuration. Then the tunnel was started and brought up to operating conditions. The motion picture camera and pressure recorder were started and the throttle closed very slowly until buzz began, at which point the throttle position was held approximately constant for a few cycles before continuing on to a lower valve opening. This procedure of a slow throttling interrupted by pauses at constant valve area was continued for the duration of the test run except for a rapid opening of the throttle at the end of the run. The tank stagnation pressure as well as the differential-gage reference pressure were recorded during the run. A no-flow pressure trace was also made after a run when possible. The differential gages and valve-position recorded were calibrated statically each day on which tests were run.

The cowling-position parameter, or angle between the axis and a ray from the cowling lip to the apex of the central body, was determined from enlargements of the no-flow motion pictures. The outlines of the conical body were extended to intersect at the apex, and then angles were measured from this point to the outline of the cowling lip. This method, however, has a low accuracy (of the order of 20 to 30 minutes) because of the presence of a slight fuzziness on the shadowgraph outlines.

The value of A_n, area of the valve opening normal to the axis, was found for each position of the throttle wheel by integrating the shadowgraphs obtained by placing the valve in the optic system with the flow axis alined with the optic axis. The value of A_n is only a relative, and by no means exact, measure of the effective throttle area since the valve seat is appreciably recessed. Consequently, the effective area is always much larger than A_n, but the variations in A_n are still indicative of variations in the effective throttle area.

RESULTS AND DISCUSSION

Comparison of Theoretical and Experimental Results

Theoretical computations of buzzing cycles for configuration I ($\theta_l = 44^\circ \pm 20'$) with duct lengths of 156 inches and 34 inches have been made. These cycles were typical of the configurations which buzzed with the vortex at the lip and, in addition, were the most complicated in the sense that the one-dimensional wave pattern included a large number of generated and reflected waves. The cycle for the 156-inch duct is discussed first because it more clearly shows the waves and their reflections since the duct is long enough to permit the complete generation of a wave before its own reflection from the nozzle exit returns to alter the generation.

The basic computations for this cycle are given in appendix B. The characteristic or wave diagram, including one space-time history for a fluid particle which enters as the buzz starts, is shown in figure 8, whereas the theoretical pressures are plotted on the experimental pressure record in figure 9. Flagged symbols are employed in this paper to denote those values computed from the experimental records. A comparison of the many additional theoretically computed points with the experimental pressure record shows generally good agreement for all five pressure traces and thus offers strong evidence that the modified theory is valid.

The lowest trace of figure 9 is that of the valve-position indicator. This is not a smooth curve because of the electrical "pickup" and, consequently, the value employed to determine A_n is the average of the maximum and minimum of that part of the trace where the "pickup" is smallest. The topmost blips indicate the timing-light flashes used to synchronize the motion pictures to the pressure record.

A strip of movie film (fig. 10) the frames of which are numbered to correspond to the numbers in the blips at the top of the pressure record (fig. 9) shows the position of the normal shock at various times. The shock moves outward between the first and second frames and then returns into the cowling between the third and fourth frames, where it remains until the fourteenth frame. Three-dimensional optical effects are responsible for the apparent presence of a normal shock ahead of the cowling in frames 4 to 13. It is evident that the flow pattern is not precisely symmetrical, a fact caused by a slight eccentricity in the location of the central body.

At a given value of x/L (in fig. 8) the increase of the characteristic parameters P or Q with time indicates the passage of a downstream or upstream compression wave, respectively. Similarly, a decrease in P or Q denotes an expansion wave.

The wave pattern of the cycle is now discernible from figures 8 to 10. The normal shock moves out because of the separation induced by the vortex and assumes a steady location on the spike which is dictated by the choking in the inlet. This motion of the shock causes an expansion wave to move downstream to reduce the mass flow. At the nozzle exit the downstream expansion is reflected as another expansion which moves upstream until it overtakes the normal shock whereupon, after a slight delay, this shock retreats into the cowling. The rearward motion of the normal shock creates a strong downstream compression wave which is closely followed by a much weaker expansion wave. This weaker expansion wave is probably due to the fact that when the shock moved into the inlet it went too far downstream. Consequently, when separation occurred behind it, the shock had to move up the channel somewhat and in so doing generated a weak expansion. In general terms, the shock overshot the equilibrium position when it moved back and, hence, had to adjust its position by moving upstream a little. It is important to note that the vortex from the intersection of the conical and normal shocks had to touch the inner wall of the cowling as the shock returned into the diffuser and yet separation did not occur to initiate the next cycle. An explanation for this phenomenon may be found in the following considerations. First, the normal shock is retreating so that the total pressure losses across it are reduced. It is then possible that inside the cowling the static pressure of the fluid on the outer side of the vortex sheet will not be required to equal its stagnation pressure; therefore, separation may be avoided (see reference 3). Second, the strong upstream expansion tends to prohibit separation by accelerating the flow and producing a favorable pressure gradient along the diffuser.

The combination of a strong compression followed by a weaker expansion is reflected as a unit, with the same sign both at the nozzle exit and at the shock inside the cowling. Each reflection, however, lessens the magnitude of the waves so that, as the pressure in the diffuser is increased by the waves, the steps due to the waves approach zero. The shape of the pressure-time curve so generated has often been described as a "relaxation type" but is, in reality, a series of step functions separated by approximately constant pressure plateaus. The compression waves eventually force the normal shock to the cowling lip where the vortex attains a position from which it can start the cycle again. In this particular cycle, the normal shock starts to move outside the cowling in the beginning of the next oscillation just prior to the arrival of the seventh upstream reflection of the compression wave which by then has degenerated from an original calculated magnitude of 4.7 pounds per square inch to only 0.1 pound per square inch. A

possible explanation for the origin of the second cycle between the two compression reflections might be that the earlier of the two waves placed the vortex from the normal shock in a position where a random motion could enable the vortex to cause separation. Another possibility might be a time lag required for the separation to grow to a value where it could choke the flow.

The magnitude of the errors which can be introduced by the various assumptions may also be determined. By using the exact formula for the variation of the characteristic parameters across a constant-pressure entropy discontinuity with the lowest value of a/a_{0_∞} occurring in the cycle, the error in the reflected value of P may be found from equations (10), (11), and the following equations (47) and (48) (which are similar in form to equation (18)):

$$Q_2 - Q_e = \frac{2}{\gamma - 1} \frac{a_e}{a_{0_\infty}} \left(e^{\frac{S_2 - S_e}{R} \frac{\gamma - 1}{2\gamma}} - 1 \right) \tag{47}$$

$$P_2 - P_e = \frac{2}{\gamma - 1} \frac{a_2}{a_{0_\infty}} \left(1 - e^{\frac{S_e - S_2}{R} \frac{\gamma - 1}{2\gamma}} \right) \tag{48}$$

This error in P is equal to 0.0019, which corresponds to a positive pressure deviation of approximately 0.1 pound per square inch. Consequently, the assumption of $\frac{a}{a_{0_\infty}} \approx 1$ and $e^{\frac{\Delta S}{R} \frac{\gamma - 1}{2\gamma}} \approx 1 + \frac{\Delta S}{R} \frac{\gamma - 1}{2\gamma}$ introduces an error no larger than 0.1 pound per square inch at each reflection and usually is considerably less since the low temperature is present for only a small part of the cycle.

The highest value of the entropy in the cycle is 0.2723; therefore, the maximum error involved by neglecting the passage of entropy discontinuities through the throat must not be greater than the value computed from equation (36), that is, $Q_q - Q_g = -0.0059$.

This neglected increment is approximately equal to an expansion wave of 0.33 pound per square inch. The entering entropy, however, drops enough in 0.015 second after the maximum so that the net value of the reflected waves then would be less than 0.1 pound per square inch. Thus, negligence of entropy has introduced a time distortion in

the wave pattern by omitting an expansion wave of 0.3 pound per square inch followed 0.015 second later by a compression wave of 0.2 pound per square inch, both of which will damp out as they reflect back and forth in the diffuser.

Since the strongest single compression in the cycle has a pressure ratio of $\frac{77.3}{72.6} = 1.065$ (see gage 4 of fig. 9 at $t \approx 0.04$), the assumption of isentropic waves is valid beyond question.

The assumption of quasi-steady flow ahead of the cowling for purposes of entropy and mass-flow computations neglects the velocity of the normal shock. From the movie film it appears that the shock velocity is about 4 feet per second, which, computed on a normal-shock basis for a free-stream Mach number of 1.90, yields a ratio of stagnation velocity of sound behind the shock to that of the free-stream stagnation sonic velocity of 1.00046 as the shock moves outward. Under these conditions, the true local entropy at the lip is greater than the steady-flow value by an increment of $\frac{\Delta S}{R} = 0.003$, and the correct mass flow is obtained by multiplying the steady-flow value by a factor of 0.999. The possibility of other waves between the cowling and shock must also be considered, but, since the time interval for flow to pass from the spike tip to the cowling is approximately 0.0001 second and none of the unsteady waves has a very large pressure slope dp/dt, these waves will also have negligible effect.

The influence of a variation in A_e or m_b/m_∞, which, of course, changes M_e, is shown by figure 11. The A_e value of 3.190 square inches used for the sample computations and comparison of theory and experiment was the channel area normal to the axis at $x = 12.75$ inches. This area is not the largest area of the diffuser, since at the end of the central-body support strut the area increases to 3.339 square inches. Thus, an effective area of 3.190 square inches presumes an average boundary-layer correction of 0.149 square inch in the remainder of the diffuser. Since there was no accurate method of measuring this correction, the influence of arbitrarily varying the effective area to 2.99 square inches was investigated. For a $\frac{m_b}{m_\infty} = 1.000$ and $A_e = 2.99$ square inches, M_e was found to be 0.163. In a similar manner as set forth in appendix B for $A_e = 3.190$ square inches, the wave diagram and pressure-time curves were determined by using the identical few experimental pressures. An examination of figure 11 shows that the only significant difference is that the pressure in the middle

part of the cycle is higher for $A_e = 2.99$ square inches than for $A_e = 3.19$ square inches and the same $\frac{m_b}{m_\infty} = 1.000$.

Also, the effect of changing the mass flow at start of buzz from $\frac{m_b}{m_\infty} = 1.000$ to $\frac{m_b}{m_\infty} = 0.985$ for an effective area $A = 3.190$ square inches was determined. This computation was complicated by the fact that it was necessary to shift from the reflection curve at the cowling lip for $\frac{m_2}{m_\infty} = 1.000$ to $\frac{m_2}{m_\infty} = \frac{m_b}{m_\infty} = 0.985$ in order to complete the cycle. These reflection curves are plotted in figure 12, along with a line between them which was arbitrarily assumed to represent conditions as the shock moves from the cowling lip out to where the buzz starts again at a mass flow of 0.985. In figure 11 the untailed diamonds represent the pressures if the ratio $\frac{m_2}{m_\infty} = 1.000$ is assumed once the shock has returned into the cowling until the next buzz starts. The tailed diamonds represent the adjustment obtained by following the path 1, 2, 3 (fig. 12) along the reflection curve at the cowling as the shock moves out. Higher pressures are evident throughout after the experimentally adjusted pressure portion of the cycle, with the cycle for $\frac{m_2}{m_\infty} = 1.000$ resulting in greater pressures than those in the cycle which allows for the mass-flow reduction from $\frac{m_2}{m_\infty} = 1.000$ to $\frac{m_2}{m_\infty} = 0.985$.

A close inspection of figures 9 and 11 reveals the fact that the theoretical pressures for $\frac{m_b}{m_\infty} = 1.000$ do not return to the original trip value of 87.0 pounds per square inch, but reach a value of only 86.7 pounds per square inch. This discrepancy probably is due to the continuous slow throttling of the exit valve, since the valve-position indicator showed a 3.4-percent decrease in A_n during the cycle from its value at the start of 0.67 square inch. Such a throttling could generate upstream compression waves to increase the experimental pressure above the theoretical value computed for constant throttle area and M_e.

The experimental pressure record also shows a pressure loss through the pipe plus an increasing hash or noise level as x/L increased. These results were to be expected since there were three 90° elbows in the standard pipe employed as a duct and in addition a chatter in the gate valve which was used as a throttle. The entropy increase along

the pipe, as well as the waves introduced by the chattering valve, of course, were neglected in theoretical work and are, therefore, another source of error.

Approximate values of the mass flow entering and leaving the ram jet are presented in figure 13. The "entering" mass-flow curve is really an extrapolated curve determined from pressures downstream which gives the mass flow behind the normal shock, and, consequently, when the normal shock is in motion inside the cowling, an error will be present. This error is evident in the apparent decrease in entering mass flow from $t = 0.036$ to $t = 0.0375$ which, in reality, is just the shock moving upstream inside the cowling after overshooting when it returned from the external spike. The mass-flow curve is therefore adjusted as shown by the dashed line to give the correct entering mass flow.

An approximation for the exit mass flow was obtained by computing the mass flow on an effective entropy basis (square symbols in fig. 13) and then correcting this value when the fluid which entered the cowling at the start of buzz had reached the exit. Each value of the mass flow at the exit at time t_1 was multiplied by a correction factor based on the entropy existing at the cowling inlet at time $t_1 - \Delta t$, where Δt was the time required for fluid to flow from the cowling to the exit at a velocity determined from the effective Mach number M_e and steady flow.

$$\Delta t = \frac{L}{M_e \frac{a_e}{a_{o_\infty}} a_{o_\infty}} = \frac{13.0}{0.1528 \times 0.99767 \times 1117.4} = 0.0763 \text{ sec} \qquad (49)$$

Integration of the area under the mass-flow curves and division by the product of mass flow at start of buzz multiplied by the cyclic time yields the average mass-flow ratio

$$\frac{\bar{m}}{m_b} = \frac{\int_o^t m(t)\, dt}{m_b t} \qquad (50)$$

A value of 0.951 is obtained for the adjusted curve for the cowling inlet and 0.953 for the nozzle exit. (If a time lag $\Delta t' = 0.083$ second, which is the time required for the initial fluid to reach the exit, is used, a value of 0.952 results at the exit.) According to these approximations, which include the mass adjustment shown by the shaded area in

figure 13, there is slightly less mass in the diffuser at the time of the start of the second cycle. This condition is a logical one, since air of higher entropy than the effective value is still flowing in the diffuser at time the second buzz starts. The assumptions made to compute the mass flow, however, are so rough that the accuracy of the third significant figure is very doubtful.

The same central body and cowling were tested with the short duct which prescribed an over-all length of 34 inches, or ratio of length to maximum internal diameter of 16.5 approximating the proportions of long ram jets. The wave diagram and the pressure record containing both theoretical and experimental points are shown in figures 14 and 15 for the fourth oscillation after starting. This oscillation was chosen because of its closer similarity to the one for the longer length in order to facilitate comparison. Since the value of p_{o_∞} for this run was 100.7 pounds per square inch absolute, compared to 101.0 pounds per square inch absolute for the longer diffuser, the value of p_b was reduced from 87.0 pounds per square inch absolute to 86.6 pounds per square inch absolute. The theoretical computations are based on $A_e = 3.190$ square inches, $\frac{m_b}{m_\infty} = 0.993$, $M_e = 0.152$, but the cycle is not, however, adjusted for the motion of the shock from $\frac{m_2}{m_\infty} = 1.000$ to $\frac{m_2}{m_\infty} = 0.993$ just prior to the next buzz. The value $M_e = 0.152$ was chosen after an initial computation employing $\frac{m_b}{m_\infty} = 1.000$ and $M_e = 0.153$ yielded results consistently low by 0.5 pound per square inch in the latter half of the cycle. The change in the cowling-lip parameter to reduce the mass flow from $\frac{m_b}{m_\infty} = 1.000$ to $\frac{m_b}{m_\infty} = 0.993$ is less than $0^\circ\ 10'$ (see fig. 25, reference 3) which is much smaller than the measurable accuracy of the parameter by the methods employed. Consequently, such an adjustment does not invalidate the solution in any way.

Again, close agreement between theory and experiment is attained. It is evident that the compression waves computed lead the experimental ones by about 0.001 second. This error is due to the initial time location of the first adjusted compression wave being in error by that amount, but, since the response of the recording apparatus was flat to only 300 cycles per second, this error was not worth correcting. The valve chatter is much more pronounced in the third trace where the pressure pickup was located only $3\frac{1}{2}$ inches ahead of the valve.

Points indicating the arrival of similar waves at gage 1 on the first trace of figures 9 and 15 are numbered to show the correspondence of the wave patterns for the long and short diffusers. The magnitude of the pressure variations is smaller for the short configuration because the reflection of the expansion wave, generated when the shock moves out to start the buzz, returns to hit the shock and stop its motion before it can move out far enough to reach a new equilibrium position on the spike. From figure 9 it is evident that the shock will move out for about 0.013 second before reaching equilibrium if its outward motion is due to vortex-induced separation and it is not forced out further by being hit by a strong compression. In contrast it takes only about 0.005 second for a wave to traverse the short duct in both directions. Consequently, for the same value of A_n, all waves have less strength for the short diffuser than for the long one. The maximum and minimum pressures for the cycles computed were 87.0 pounds per square inch and 72.6 pounds per square inch in the long configuration contrasted to 86.6 and 79.0 in the short one. Similarly, the minimum entering mass flow, referred to free-stream cowling area, was 51 percent and 79 percent for the long and short diffusers, respectively.

The motion-picture film (fig. 16) taken concurrently with the pressure record and numbered to correspond to the numbers on the pressure record shows the shock motion to be much smaller for the short pipe than for the long one. The shock motion also agrees with the theory in every respect.

The curves of mass flow against time (fig. 17) were computed by the same method employed previously. The ratio of average mass flow to mass flow at start of buzz is 0.979 at entrance and 0.977 at exit. The entering value was not adjusted for the motion of the shock from $\frac{m_2}{m_\infty} = 1.000$ to $\frac{m_b}{m_\infty} = 0.993$ prior to the next cycle which would reduce the average entering value slightly. The ratios of the average mass flows to the mass flow based on 100 percent capture area $\frac{\overline{m}}{m_\infty}$ are 0.972 and 0.970, respectively, compared with 0.951 and 0.953 for the longer diffuser.

Since all the variations in p, a, S/R, and so forth are smaller for the shorter pipe, the errors introduced by the various assumptions (except the one made by concentrating the area changes) which simplify the exact one-dimensional theory are less than those for the longer pipe. The distortion in the wave pattern due to assuming that all the area changes are concentrated at the inlet and exit is increased in the smaller diffuser since the actual area variations occupy a larger percentage of the total length. (See fig. 6.)

General Nature of the Buzz Cycles

The manner in which the cyclic period is usually changed due to throttle adjustment is shown in figure 18, which is another part of the pressure record for configuration I, $\theta_l = 44^\circ$, L = 156 inches. At point I (see fig. 18(a)) the "basic cycle" is (1) a downstream expansion, (2) an expansion reflected upstream from the exit which pulls the normal shock back in, (3) a downstream compression, and (4) a reflected upstream compression which forces the shock out to start the next cycle. Two smaller compressions are superimposed on the basic cycle, since the strong upstream compression which starts the next cycle passes through the contraction at the cowling entrance and reflects a weaker compression which shows up in points 1, 2, and 3. This is, in turn, reflected and re-reflected as a compression upstream from the exit, points 4 and 5, downstream from the cowling contraction, points 5 to 7, and finally upstream again, points 8 to 10. Further reflections are negligible.

As the throttle is opened, the reflections from the throttle become smaller. This phenomenon is due to that fact that, if the conditions h, j, and k represent, respectively, the conditions ahead of a downstream wave, behind the downstream wave, and after the upstream reflection of the wave from a sonic valve, the ratio of the wave strengths for isentropic waves is by linearization approximately

$$\frac{p_k}{p_j} \doteq 1 + \left(\frac{p_j}{p_h} - 1\right)\left(\frac{p_h}{p_j}\right)^{\frac{\gamma-1}{2\gamma}} \frac{\frac{2}{\gamma - 1} - M_h}{\frac{2}{\gamma - 1} + M_h} \tag{51}$$

As the sonic area is increased, the Mach number M_h must increase since the ratio of the sonic throat area to A_h becomes larger and the reflected pressure wave becomes weaker $\left(\frac{p_k}{p_j}\right.$ approaches 1.0$\left.\right)$.

If each reflection becomes weaker while the strength of the initial expansion remains approximately constant, it will take an increasing number of compression reflections to move the normal shock to a point where the vortex starts the next cycle. Figure 18(b) shows this clearly. Region I requires only one compression reflection; whereas regions II, III, IV, and V require two, three, four, and five compression reflections, respectively. In some cases it is evident that the cycle starts between reflections and, as explained earlier, starting at this time is probably due to the previous wave moving the normal shock to a position where the vortex is on the verge of causing separation so that any random

variation in the flow starts the cycle. Note that the basic cycle is approximately the same for all the frequencies and that the minor compression wave becomes unnoticeable as the valve is opened.

The pressure record obtained when the valve was quickly opened for the short diffuser (fig. 19) has similar characteristics. The waves, however, are not as sharply defined as in the longer pipe.

The short duct shows a marked decrease in the wave amplitude as the valve was opened. The magnitude of the upstream compression which knocks the shock out of the cowling determines the expansion strength, since a strong compression will knock the shock further out before it can be stopped by the reflected expansion. In the longer pipe, however, (fig. 18) the amplitude varied only slightly, since the normal shock moves out until it reaches an equilibrium with the separation-choked cowling before any of the reflected expansion returns to alter its motion.

An over-all examination of the results of the nine different supersonic-inlet geometries tested revealed a general behavior pattern for the buzzing after it was once initiated. This result was true although the 30° configurations were always choked at the cowling inlet so that the normal shock could not enter during steady flow. Also, configuration II for $\theta_l = 39^\circ\ 50'$ buzzed due to the vortex from the separation-induced lambda shock striking the cowling.

The pressure records for configuration III were very similar to those shown for configuration I $\theta_l = 44^\circ$ after the cycle in which the shock motion first became appreciable. This cycle was usually preceded by a few short oscillations of much lower magnitude.

The pressure records for configuration II were similar to those for configurations I and III only after the amplitude of the buzz had become large enough for the basic cycle to manifest itself. With this body and $\theta_l = 43^\circ\ 10'$, the buzz did not start until the normal shock was appreciably more than halfway out on the spike and the vortex appreciably inside the cowling. The buzz then began in a manner best described as an unstable organ-pipe type of resonance. As evident from figure 20, the oscillations in the short diffuser increased in amplitude rapidly and then remained constant. Moving pictures showed that the buzz was not started by any vortex action, but rather by a boundary-layer instability, and that the magnitude of the oscillations built up until the normal shock was moving from a point one-quarter of the way down the spike to a point off the spike ahead of the tip. Shadowgraph excerpts (the frames are numbered to correspond to the numbers in fig. 20) of this configuration are shown in figure 21. The table on the following page gives the difference in pressures from the peak to the valley at each of the

three pressure pickups at times I, II, and III for three consecutive oscillations noted in figure 20:

Time	Δp for (psi)		
	gage 1, $\frac{x}{L} = 0.338$	gage 2, $\frac{x}{L} = 0.721$	gage 3, $\frac{x}{L} = 0.897$
I	7.7	10.7	12.5
II	9.5	13.1	14.7
III	11.0	15.6	18.2

This table definitely refutes the use of a Helmholtz resonator analysis even for this cycle, which in the absence of starting due to the vortex is nearest to a sinusoidal cycle, and hence would be most favorable to Helmholtz theory. At the same time, it substantiates the plane-wave theory for the short diffuser having a fineness ratio of less than 17. The basis for this conclusion may be found in the primary assumptions employed in the Helmholtz derivation; namely, the pressure is uniform at any time in the large cavity, and thus the pressure fluctuations must have the same magnitude throughout the cavity. The pressure records, however, show that in the duct, which in the Helmholtz analysis (reference 5) is considered the resonator cavity, the magnitude of the fluctuations varies by about 50 percent in the same cycle. Furthermore, although the oscillation is unstable and is increasing rapidly, the pressure variation near the valve $\left(\frac{x}{L} = 0.897\right)$ during one cycle is still larger than the pressure variation further upstream $\left(\frac{x}{L} = 0.338\right)$ during the next cycle. In other words, the diffuser behaves similarly to an organ pipe with relative nodes in velocity and anti-nodes in pressure at the exit for this cycle. Additional verification was obtained from the longer version of the same supersonic-diffuser configuration where a typical oscillation generated a pressure variation of 1.2 pounds per square inch at $\frac{x}{L} = 0.074$; whereas at $\frac{x}{L} = 0.705$ the variation was 4.5 pounds per square inch.

Figure 20 also is an exception to the general trend of increasing frequency with decreasing valve area since the periodic time increases from 0.0149 second to 0.0155 second during resonance. The reason for this result is found in the "inertia" effects of the external motion of the shock. From figures 14 and 16 it is obvious that the shock does

not start to return to the cowling as soon as struck by the upstream expansion wave (t = 0.0114 second, frame 5) but delays before starting inward (t = 0.0152 second, frame 7). As the amplitude of the shock motion increases, more of the expansion will have to strike it to initiate its movement toward the cowling. Thus, for figure 20, the periodic time, comprised of the lag time and basic cycle time (that is, that time required for an expansion and compression to traverse the duct in both directions), increases as the amplitude and lag increase.

It is then obvious that, for any finite-amplitude oscillation governed by reflections from the exit, the periodic time must be greater than the basic cycle interval. The minimum period for the configurations tested was 0.0148 second, with a basic cycle time of 0.0101 second, when waves reflected from the exit controlled the buzz. Configuration II, $\theta_l = 36^\circ\ 50'$, however, oscillated at a very high frequency with a period of approximately 0.002 second when the exit area was reduced appreciably. This oscillation may have been governed by the supersonic diffuser entirely and perhaps resulted from the periodic boundary-layer variations passing through the first minimum.

A Possible Application to Simulate Constant-Area Heat Addition By Cold Flow With Area Contraction

Once the quasi-one-dimensional nature of the wave phenomena has been established, the possibility arises of employing area changes to simulate heat addition. An examination of equations (1) and (2) shows that the parameters P and Q are functions only of the changes in A or S/R. It is possible therefore to get the same variation for one (not both simultaneously) of these parameters due to a change in S/R while A is held constant that can be obtained by holding S/R constant and varying A. A generalization of this principle is used to produce theoretically a similar wave pattern for the case of constant-area heat addition and isentropic area contraction for configuration pairs like those shown in figure 22.

Consider the simplified combustion process in a semi-infinite pipe diagrammed in figure 22(a) where the combustion is assumed to occur in a discontinuous flame front. If conditions at the flame front may be assumed to reach a steady or equilibrium flow after each transmission and reflection of a pressure wave, the equations of continuity, energy, momentum, and state may be incorporated in a trial-and-error process to determine the waves transmitted and reflected for each incident wave. (The exact characteristic equations cannot be used since the derivatives become infinite at the discontinuity.) Of course, an assumption regarding

the amount of energy added per unit mass flow must be made for the energy equation. This assumption is a very difficult assumption to make since the waves change the Reynolds number, velocity, and air-fuel ratio at the combustion zone.

Two very simple assumptions were used for the two illustrative computations; namely, (1) the ratio of total temperature across the flame front was constant, and (2) the energy added per unit mass was constant. For an initial Mach number of 0.200 ahead of the flame and 0.400 behind it, these assumptions prescribed a constant stagnation-temperature ratio of 3.0482 for the first case and an increment in stagnation temperature of 2.0482 times the initial, undisturbed, stagnation temperature for the second case. A downstream-moving expansion was then assumed to strike the flame and theoretical computations made for the wave pattern due to the reflections and re-reflections from the flame discontinuity and nozzle. Under the limitation of a choked exit nozzle the waves rapidly damped out. The general form of the wave diagram is shown by the solid lines of figure 23 and the corresponding pressure-time curve at $x = x_1$ (located ahead of the flame by an amount equal to one-half the distance from the flame to the nozzle) for three different initial expansion strengths is plotted in figure 24.

Computations were then made for a discontinuity in area in place of the flame front with the requirements that: (1) undisturbed conditions ahead of the discontinuity be identical to those for the heat addition, and (2) the medium-strength expansion have the same first upstream reflection for both the area change and heat addition. By trial and error the area ratio corresponding to the constant-stagnation-temperature ratio was found to be 0.5129 and that for the constant increment in stagnation temperature to be 0.3801. The length of the system after the discontinuity in area change was determined so that an infinitesimal disturbance would require the same amount of time to travel from the discontinuity to the exit nozzle and back to the discontinuity for both the heat addition and contraction cases. In other words, if ϵ_α denotes the distance from the flame front to the nozzle and ϵ_β the distance from the area change to the nozzle (see fig. 22),

$$\Delta t = \epsilon_\alpha\left(\frac{1}{a_\alpha + u_\alpha} + \frac{1}{a_\alpha - u_\alpha}\right) = \epsilon_\beta\left(\frac{1}{a_\beta + u_\beta} + \frac{1}{a_\beta - u_\beta}\right) \tag{52}$$

$$\frac{\epsilon_\beta}{\epsilon_\alpha} = \frac{\dfrac{1}{a_\alpha + u_\alpha} + \dfrac{1}{a_\alpha - u_\alpha}}{\dfrac{1}{a_\beta + u_\beta} + \dfrac{1}{a_\beta - u_\beta}} \tag{53}$$

The rest of the wave pattern until damping was completed was then computed under the same restrictions as imposed on the heat-addition solution. Good agreement is shown in figure 24 for the pairs of pressure-time curves for the corresponding conditions of (1) total temperature ratio equal to 3.0482 and area ratio of 0.5129, or (2) total temperature increment of 2.0482 and area ratio of 0.3801. For each of the three initial expansions, all the curves except that for the constant ΔT_o will damp to the same final pressure (which is, of course, different for each expansion) and return to the original Mach number of 0.200 ahead of the discontinuity. Thus, for either of the heat-addition assumptions made, a corresponding area change could be employed.

When the amplitude of the buzz in an actual ram jet is small, the variation of Reynolds number, velocity, and air-fuel ratio is also small. In a ram jet, however, there is also the added complication of coupling between the fuel-injection nozzles and the combustion zone whereby a wave originating from the combustion zone travels upstream with a velocity $a - u$ to the fuel-injection system and changes the air-fuel ratio of the fluid present at the fuel nozzles. This fluid then travels downstream with a velocity u to the combustion zone where the new air-fuel mixture burns to generate a new wave. This phenomenon cannot be duplicated by waves whose speed is strictly limited to the local sonic velocity superimposed on the local fluid velocity. If the reflections from the shock at the inlet, from the nozzle exit, and from the waves striking the flame front, however, have a stronger influence on the pressure pattern than the waves generated by the change in air-fuel ratio, there is the possibility that the combustion in a particular buzzing ram jet may follow approximately a law of energy release which can be simulated by an area change. In that case the actual ram jet (fig. 22) with a finite combustion zone might be tested for its behavior during buzz by the cold-flow test of the configuration (fig. 22) in which the combustion chamber is replaced by a shorter section with a gradual area reduction.

CONCLUDING REMARKS

Experimental instantaneous pressure records of simulated ram-jet models without heat addition showed that these models buzzed in a manner governed internally by quasi-one-dimensional (plane-wave) unsteady-flow theory and not in accord with an analysis of the problem by the laws of Helmholtz resonator theory. A theory applicable to the buzzing problem was obtained through modification of the one-dimensional, unsteady-flow theory by introducing specified assumptions which greatly facilitated the computational efforts without impairing the usefulness of the theory for this flow. Because of the difficulty in computing the three-dimensional, unsteady, viscous flow when the shock was in motion ahead

of the cowling and in computing when the shock was in motion far from equilibrium with the waves moving upstream from the nozzle, it was necessary to use a few experimental points at the start of the cycle as a basis on which to compute the remaining pressure points of the cycle. Theoretical computations of the pressure-time curves, which were made on this basis for one supersonic-diffuser configuration with two different subsonic-duct lengths, agreed closely with the experimental records. The entrance and exit mass-flow - time curves, as well as the wave diagrams, were also computed for these configurations by the unsteady-flow theory.

The wave pattern causing the buzz was found to be a basic cycle which consisted of a downstream expansion reflected at the exit as an upstream expansion and a downstream compression reflected as an upstream compression plus a variable number of compression-expansion couplets following the basic cycle. The number of compression-expansion couplets depended on the valve-exit area and decreased as this area decreased; therefore, the frequency generally increased as the throttle was closed.

The simulation of combustion in a ram jet by an area contraction for buzzing tests was discussed as a possible extension of the results.

Langley Aeronautical Laboratory,
National Advisory Committee for Aeronautics,
Langley Field, Va., January 29, 1952.

APPENDIX A

DERIVATION OF CHARACTERISTIC EQUATIONS

The general form of the quasi-one-dimensional continuity equation is expressed as follows:

$$\frac{\partial}{\partial t}(\rho A) + \frac{\partial}{\partial x}(\rho u A) = 0 \tag{54}$$

where the area A is considered to be a function of both time and position. With this equation, cases of a boundary layer growing with time as well as continued throttling may be treated. Equation (54) may be written in another form as

$$\frac{\partial \log_e A}{\partial t} + u \frac{\partial \log_e A}{\partial x} + \frac{\partial \log_e \rho}{\partial t} + u \frac{\partial \log_e \rho}{\partial x} + \frac{\partial u}{\partial x} = 0 \tag{55}$$

The following two identities

$$a^2 \equiv \gamma RT \tag{56}$$

$$d\frac{S}{R} \equiv \frac{d}{RT}(\text{heat added}) \tag{57}$$

are now introduced. The quantity a in equation (56) is the speed of an isentropic wave of infinitesimal strength, or sound wave, which may move through a fluid of varying entropy. The "heat added" of equation (57) includes the heat due to convection, dissipation, and sources. When the energy equation

$$d(\text{heat added}) = C_v\, dT - \frac{p}{\rho^2}\, d\rho \tag{58}$$

and the equation of state

$$p = \rho RT \tag{59}$$

are combined with equations (56) and (57), the differential equations between the properties of state and the nondimensional entropy are determined

$$d\frac{S}{R} = \frac{2C_v}{R} d \log_e a - d \log_e \rho \tag{60}$$

$$d\frac{S}{R} = \frac{2C_p}{R} d \log_e a - d \log_e p \tag{61}$$

Although these relationships were derived for a particular elemental volume of fluid, they also are true for all the various parts of the fluid and may be used when going from one part of the fluid to another. This procedure is justified because the entropy is a property of state so that $S(x,t) = S\left[p(x,t), \rho(x,t), a(x,t)\right]$ if all the fluid was originally in the same state. Consequently, the following partial derivatives may be obtained:

$$\frac{\partial \log_e \rho}{\partial x} = \frac{2C_v}{R}\frac{\partial \log_e a}{\partial x} - \frac{\partial \frac{S}{R}}{\partial x} \tag{62}$$

$$\frac{\partial \log_e \rho}{\partial t} = \frac{2C_v}{R}\frac{\partial \log_e a}{\partial t} - \frac{\partial \frac{S}{R}}{\partial t} \tag{63}$$

$$\frac{\partial \log_e p}{\partial x} = \frac{2C_p}{R}\frac{\partial \log_e a}{\partial x} - \frac{\partial \frac{S}{R}}{\partial x} \tag{64}$$

$$\frac{\partial \log_e p}{\partial t} = \frac{2C_p}{R}\frac{\partial \log_e a}{\partial t} - \frac{\partial \frac{S}{R}}{\partial t} \tag{65}$$

The momentum equation

$$\frac{\partial u}{\partial t} + u\frac{\partial u}{\partial x} + \frac{1}{\rho}\frac{\partial p}{\partial x} = 0 \tag{66}$$

becomes equation (67) upon insertion of equations (56) and (59)

$$\frac{\partial u}{\partial t} + u \frac{\partial u}{\partial x} + \frac{a^2}{\gamma} \frac{\partial \log_e p}{\partial x} = 0 \tag{67}$$

Substitution of equation (64) into equation (67) and simplifying yields

$$\frac{\partial u}{\partial t} + u \frac{\partial u}{\partial x} + \frac{2C_v}{R} a \frac{\partial a}{\partial x} - \frac{a^2}{\gamma} \frac{\partial \frac{S}{R}}{\partial x} = 0 \tag{68}$$

since $\gamma = \frac{C_p}{C_v}$.

Similarly, substitution of equations (62) and (63) into equation (55) results in:

$$a \frac{\partial \log_e A}{\partial t} + au \frac{\partial \log_e A}{\partial x} + \frac{2C_v}{R} \frac{\partial a}{\partial t} - a \frac{\partial \frac{S}{R}}{\partial t} + \frac{2C_v}{R} u \frac{\partial a}{\partial x} - au \frac{\partial \frac{S}{R}}{\partial x} + a \frac{\partial u}{\partial x} = 0 \tag{69}$$

Addition of equations (68) and (69) and then rearrangement yields

$$\frac{\partial}{\partial t}\left(\frac{2C_v}{R} a + u\right) + (u + a)\frac{\partial}{\partial x}\left(\frac{2C_v}{R} a + u\right) =$$

$$-a\left(\frac{\partial \log_e A}{\partial t} + u \frac{\partial \log_e A}{\partial x}\right) + \frac{\gamma - 1}{\gamma} a\left(\frac{\partial \frac{S}{R}}{\partial t} + u \frac{\partial \frac{S}{R}}{\partial x}\right) + \frac{a}{\gamma}\left[\frac{\partial \frac{S}{R}}{\partial t} + (u + a)\frac{\partial \frac{S}{R}}{\partial x}\right] \tag{70}$$

Similarly, subtraction of equation (68) from equation (69) and rearrangement gives

$$\frac{\partial}{\partial t}\left(\frac{2C_v}{R}\,a - u\right) + (u - a)\frac{\partial}{\partial x}\left(\frac{2C_v}{R}\,a - u\right) =$$

$$-a\left(\frac{\partial \log_e A}{\partial t} + u\,\frac{\partial \log_e A}{\partial x}\right) + \frac{\gamma - 1}{\gamma}\,a\left(\frac{\partial \frac{S}{R}}{\partial t} + u\,\frac{\partial \frac{S}{R}}{\partial x}\right) + \frac{a}{\gamma}\left[\frac{\partial \frac{S}{R}}{\partial t} + (u - a)\frac{\partial \frac{S}{R}}{\partial x}\right] \tag{71}$$

The following identities are used:

(1) Convective derivative $\frac{D}{Dt} \equiv \frac{\partial}{\partial t} + u\,\frac{\partial}{\partial x}$ (72)

(2) Total derivative along a characteristic of slope $\frac{dx}{dt} = u \pm a$,

$$\frac{\delta}{\delta t} = \frac{\partial}{\partial t} + (u \pm a)\frac{\partial}{\partial x} \tag{73}$$

(3) $P \equiv \frac{2}{\gamma - 1}\frac{a}{a_{o_\infty}} + \frac{u}{a_{o_\infty}} = \frac{2C_v}{R}\frac{a}{a_{o_\infty}} + \frac{u}{a_{o_\infty}}$

(4) $Q \equiv \frac{2}{\gamma - 1}\frac{a}{a_{o_\infty}} - \frac{u}{a_{o_\infty}} = \frac{2C_v}{R}\frac{a}{a_{o_\infty}} - \frac{u}{a_{o_\infty}}$

Insertion of these terms in equations (70) and (71) gives the characteristic equations in their final form

$$\frac{\delta P}{\delta t} = -\frac{a}{a_{o_\infty}}\frac{D \log_e A}{Dt} + \frac{\gamma - 1}{\gamma}\frac{a}{a_{o_\infty}}\frac{D \frac{S}{R}}{Dt} + \frac{1}{\gamma}\frac{a}{a_{o_\infty}}\frac{\delta \frac{S}{R}}{\delta t}$$

$$\frac{\delta Q}{\delta t} = -\frac{a}{a_{o_\infty}}\frac{D \log_e A}{Dt} + \frac{\gamma - 1}{\gamma}\frac{a}{a_{o_\infty}}\frac{D \frac{S}{R}}{Dt} + \frac{1}{\gamma}\frac{a}{a_{o_\infty}}\frac{\delta \frac{S}{R}}{\delta t}$$

APPENDIX B

COMPUTATION FOR CONFIGURATION I, $\theta_l = 44^\circ$, SUPERSONIC DIFFUSER WITH OVERALL RAM-JET LENGTH OF 156 INCHES

The first step in the computation for configuration I, $\theta_l = 44^\circ$, supersonic diffuser with overall ram-jet length of 156 inches is the solution of the following equation (which is the same as equation (43) of the text)

$$M_e\left(1 + \frac{\gamma - 1}{2} M_e^2\right)^{\frac{1}{2}} = M_\infty \left(\frac{p_{o_\infty}}{p_e}\right)_b \left(\frac{A_i}{A_e}\right)\left(\frac{m_b}{m_\infty}\right)\left(1 + \frac{\gamma - 1}{2} M_\infty^2\right)^{-\frac{\gamma+1}{2(\gamma-1)}}$$

For the effective area A_e, the value of the area at $x = 12.75$ inches is chosen; this area is equal to the area of the annulus formed by the inside of the pipe, which forms the principal part of the diffuser, and by the supporting strut for the central body which extends to $x \approx 15.5$ inches (fig. 5)

$$A_e = \frac{\pi}{4}\left(2.062^2 - 0.436^2\right) = 3.190 \tag{72}$$

Also, since to the order of accuracy of the "no-flow" shadowgraph measurements (fig. 25 of ref. 3), the buzz should start at a mass-flow ratio $\frac{m_b}{m_\infty} = 1.000$ because the conical shock falls on the cowling lip. When these values are used with $\gamma = 1.400$ plus the measured values of $A_i = \frac{\pi}{4}(1.2)^2$ square inches, $p_e = 87.0$ pounds per square inch absolute (fig. 9), $p_{o_\infty} = 101$ pounds per square inch absolute (recorded during test), and the nozzle Mach number $M_\infty = 1.90$, equation (43) can be solved for $M_e = 0.1528$. The effective entropy $\frac{S_e}{R}\left(\text{based on } \frac{S_\infty}{R} = 0\right)$ is determined from the assumption of steady flow just prior to the start of buzz; thus, since the above data yield an effective stagnation pressure in the duct at start of buzz of 88.4 pounds per square inch absolute

$$\frac{S_b}{R} = \frac{S_e}{R} = -\log_e \frac{88.4}{101} = 0.1332 \tag{73}$$

Similarly,

$$\frac{a_b}{a_{o_\infty}} = \left(1 + \frac{\gamma - 1}{2} \times 0.1528^2\right)^{-\frac{1}{2}} = 0.99767 \tag{74}$$

$$\frac{u_b}{a_{o_\infty}} = 0.1528 \times 0.99767 = 0.15244 \tag{75}$$

which yield starting values of the parameters P and Q

$$P_b = 5.1408 \tag{76}$$

$$Q_b = 4.8359 \tag{77}$$

The reflection curve (solid line in fig. 25) for the entrance is computed as set forth in the theoretical section by adjusting the quasi-steady values of P_2 and Q_2 by a factor which is a function of the difference $\frac{S_2}{R} - 0.1332$. Reflections at the nozzle exit are specified by the relationship $Q_3 = \frac{5 - M_e}{5 + M_e} P_3 = 0.94069P_3$ (dashed line in fig. 25). The final curve (fig. 26) needed for the completion of the wave diagram is the pressure - sonic-speed curve $\frac{p}{87.0} = \left(\frac{a/a_{o_\infty}}{0.99767}\right)^7$ (see equation 21).

Experimental values, designated by the flagged symbols on the pressure record (fig. 9) and wave diagram (fig. 8), are used to determine the downstream-moving waves when the normal shock is in rapid motion or ahead of the cowling. A linear interpolation of the variation of the parameters P and Q is assumed for all waves.

The remainder of the wave diagram is constructed by the two reflection curves and then the pressures found on the third curve from the local sonic velocity $\frac{a}{a_{o_\infty}} = \frac{P + Q}{10}$.

Approximate values of the entropy at the entrance may be found from the quasi-steady flow to the inlet when the shock is ahead of the cowling. Consider the conditions existing (fig. 8) at $t = 0.0193$ at the entrance

where $P = 5.0061$ and $Q = 4.8359$ so that $\frac{u}{a_{o_\infty}} = 0.0851$, $\frac{a}{a_{o_\infty}} = 0.98420$ (in the imaginary lamina) and $p = 79.10$. The quasi-steady-flow energy equation gives the actual $\frac{a}{a_{o_\infty}} = 0.999275$ and, since at a free-stream Mach number of 1.90, $p_\infty = 15.07$ for $p_{o_\infty} = 101.0$, and $\frac{a_\infty}{a_{o_\infty}} = 0.76205$,

$$\frac{S_2 - S_\infty}{R} = \frac{2\gamma}{\gamma - 1} \log_e \frac{0.999275}{0.98420} - \log_e \frac{79.10}{15.07} = 0.2390 \qquad (78)$$

The linearized approximation might be used instead to obtain the value of $\frac{S_2}{R}$.

$$\frac{S_2 - S_\infty}{R} = \frac{S_2 - S_e}{R} + \frac{S_e - S_\infty}{R} = \frac{2\gamma}{\gamma - 1} \frac{\Delta a}{a} + 0.1332$$

$$= 7 \frac{0.9993 - 0.9842}{0.9993} + 0.1332 = 0.1058 + 0.1332 = 0.2390 \qquad (79)$$

The ratio of the instantaneous entering mass flow to the mass flow at start of buzz is then, from equation (29):

$$\frac{m_2}{m_b} = \left(\frac{5.0061 + 4.8359}{5.1408 + 4.8359}\right) \frac{5.0061 - 4.8359}{5.1408 - 4.8359} \left(1 - \frac{0.1058}{3.5}\right) = 0.506 \qquad (80)$$

REFERENCES

1. Oswatitsch, Kl.: Der Druckrückgewinn bei Geschossen mit Rückstossantrieb bei hohen Überschallgeschwindigkeiten (Der Wirkungsgrad von Stossdiffusoren). Bericht Nr. 1005, Forsch. und Entwick. des Heereswaffenamtes (Göttingen), 1944. (Available in English translation as NACA TM 1140.)

2. Connors, James F.: Effect of Ram-Jet Pressure Pulsations on Supersonic-Diffuser Performance. NACA RM E50H22, 1950.

3. Ferri, Antonio, and Nucci, Louis M.: The Origin of Aerodynamic Instability of Supersonic Inlets at Subcritical Conditions. NACA RM L50K30, 1951.

4. Dailey, C. L.: Development of Supersonic Ramjet Diffusers. USCAL Rep. 8-1, Univ. Southern Calif., Aero. Lab., Jan. 10, 1951.

5. Sterbentz, William H., and Evvard, John C.: Criterions for Prediction and Control of Ram-Jet Flow Pulsations. NACA RM E51C27, 1951.

6. Kahane, A., and Lees, Lester: Unsteady One-Dimensional Flows With Heat Addition or Entropy Gradients. Jour. Aero. Sci., vol. 15, no. 11, Nov. 1948, pp. 665-670.

7. Ferri, Antonio: Elements of Aerodynamics of Supersonic Flows. The Macmillan Co., 1949.

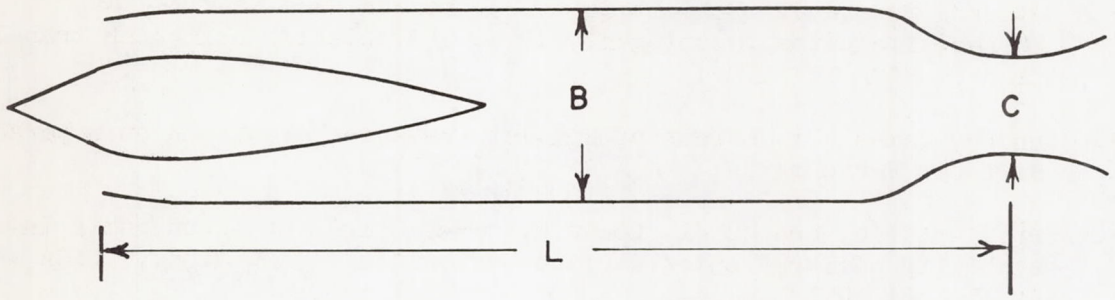

(a) Typical ram jet.

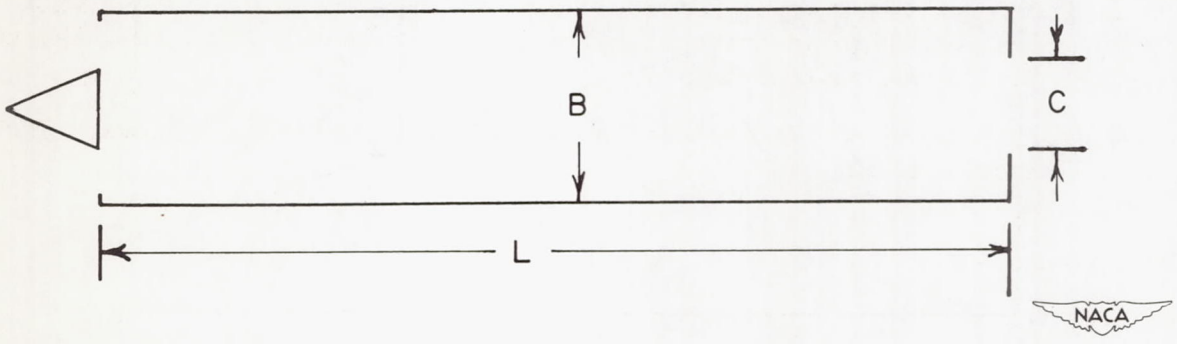

(b) Simplified ram jet assumed for one-dimensional, unsteady-flow analysis.

Figure 1.- Sketch of typical ram jet and simplified one-dimensional counterpart.

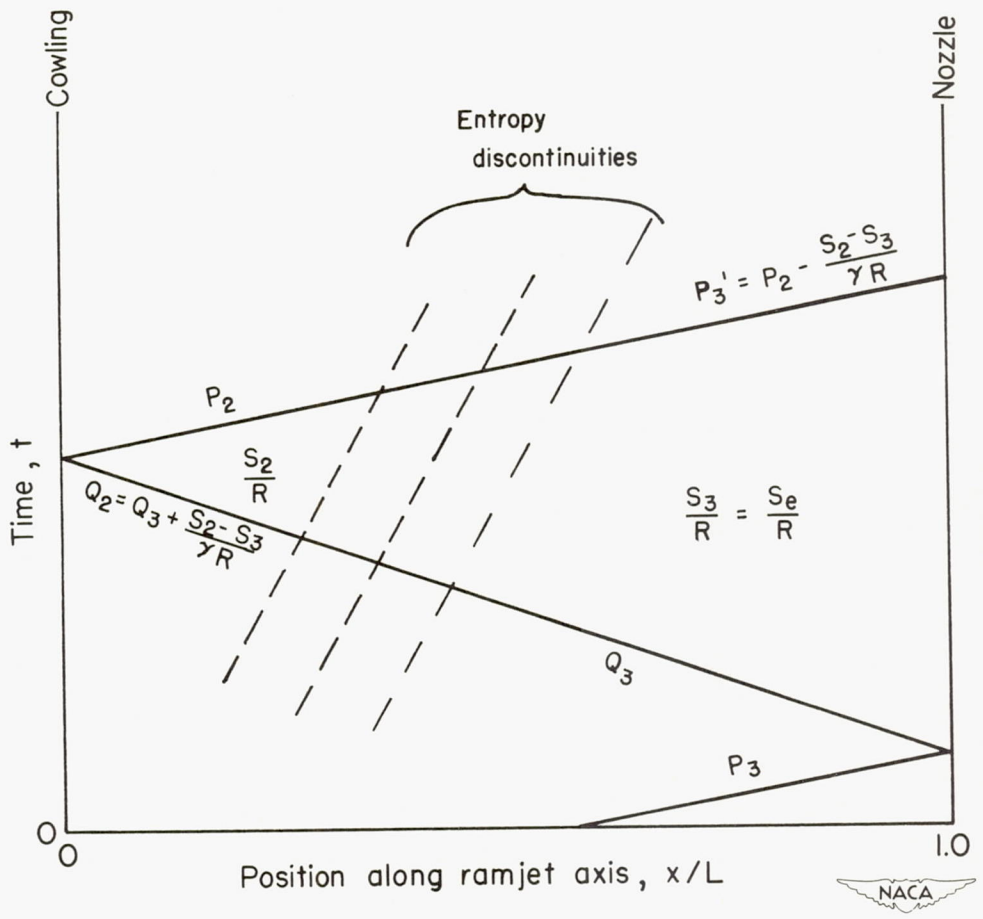

Figure 2.- Method employing quasi-steady flow values (P_2, Q_2) at cowling inlet to obtain value of P_3' reflected from shock by Q_3.

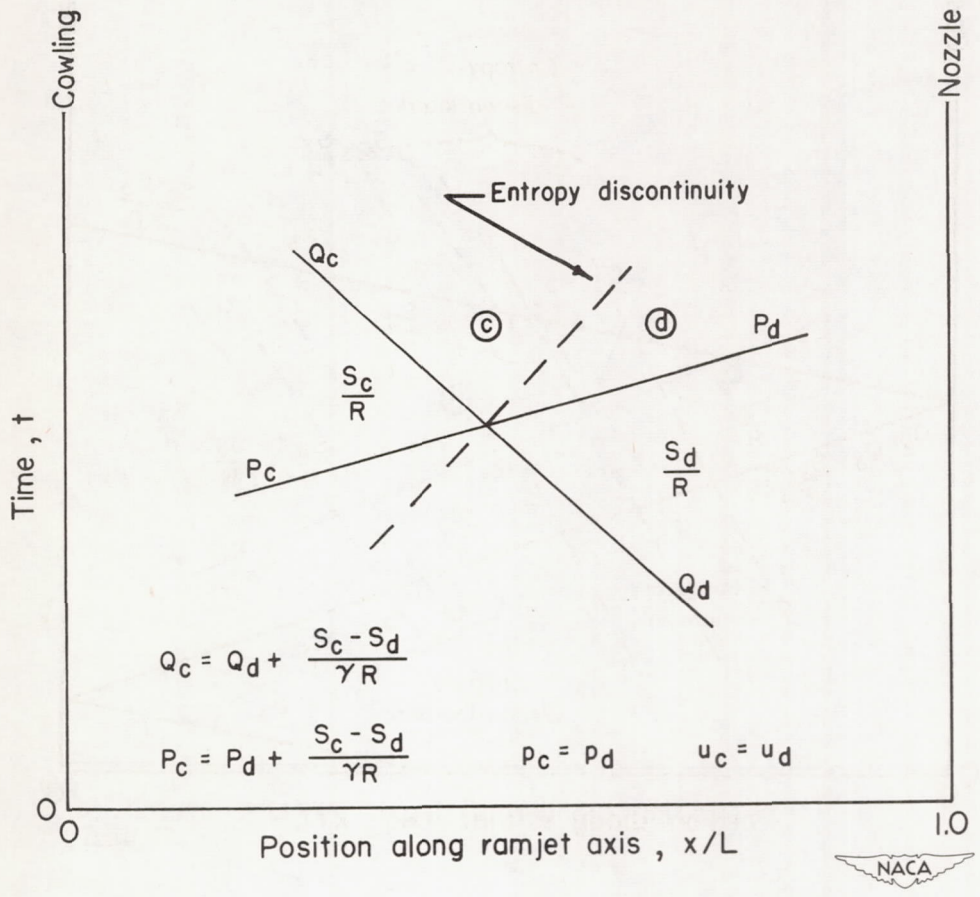

(a) Variation of parameters across an entropy discontinuity where pressure and velocity are constant.

Figure 3.- Diagrams showing how characteristic parameters P and Q may be referred to effective entropy by insertion of imaginary lamina of fluid in the flow field.

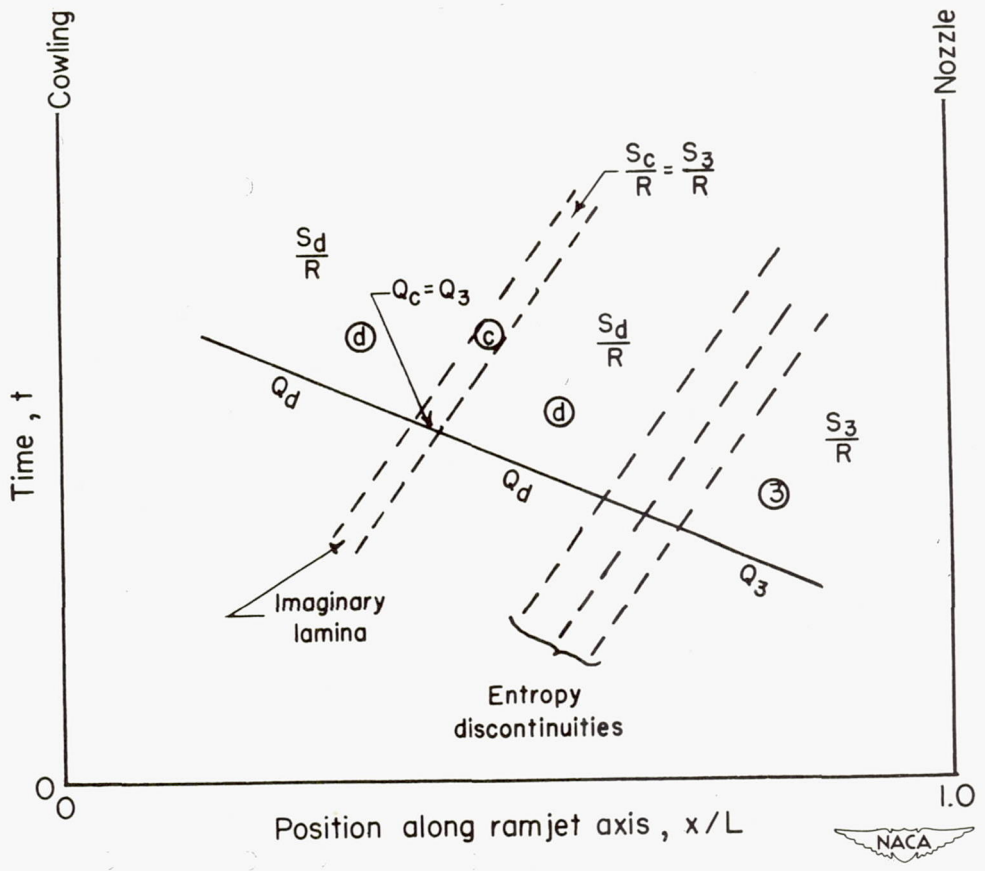

(b) Insertion of imaginary lamina of fluid (c) with entropy S_3/R into flow (d) of different entropy returns parameters to value existing originally in state (3) to permit calculation of pressure and velocity.

Figure 3.- Concluded.

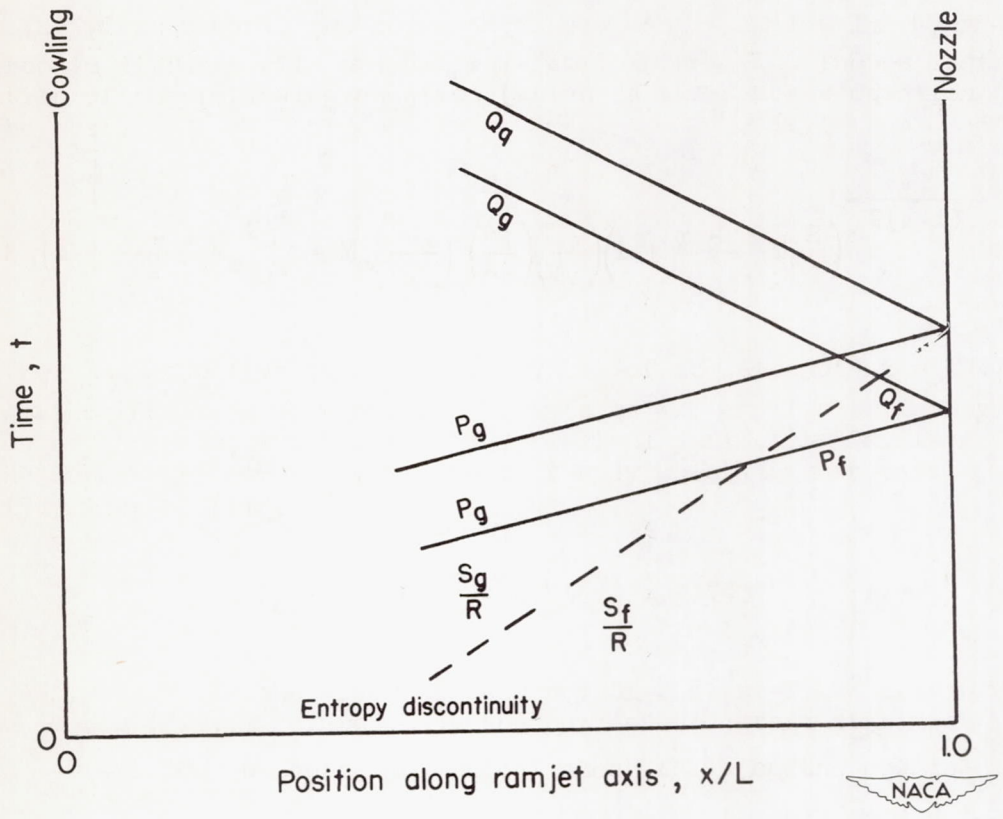

Figure 4.- Wave generated by passage of entropy discontinuity through exit nozzle.

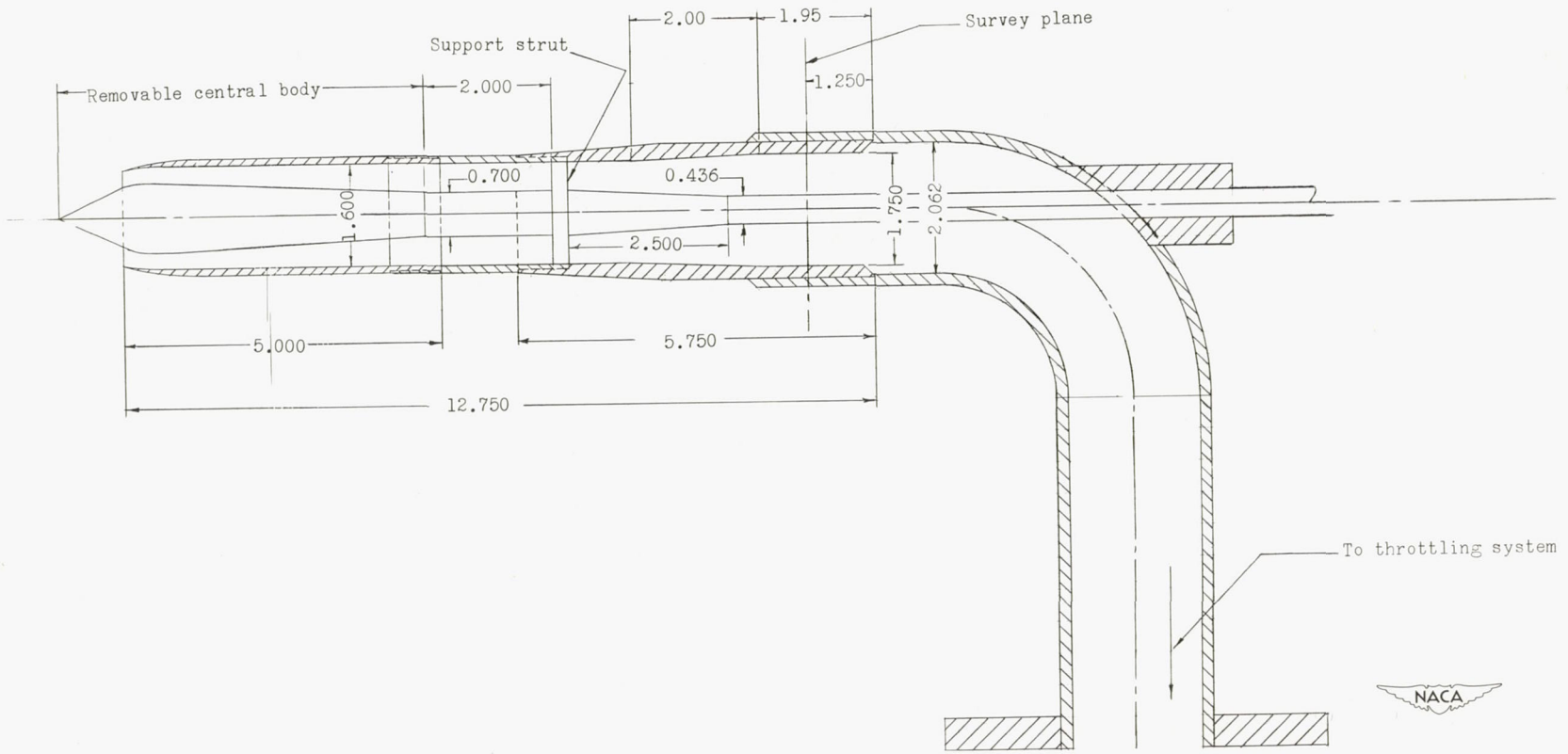

Figure 5.- General configuration of models tested. All dimensions are in inches.

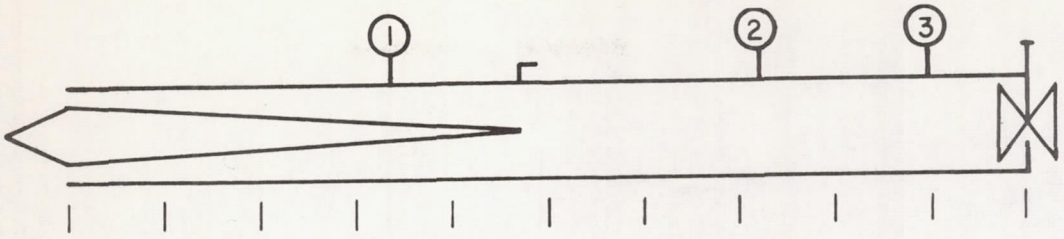

(a) Short diffuser; L = 34 inches.

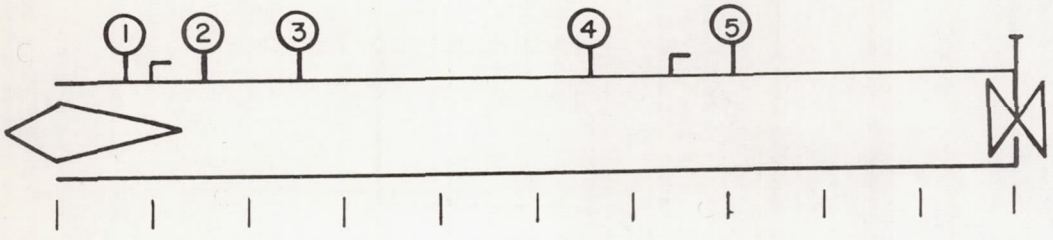

(b) Medium diffuser; L = 156 inches.

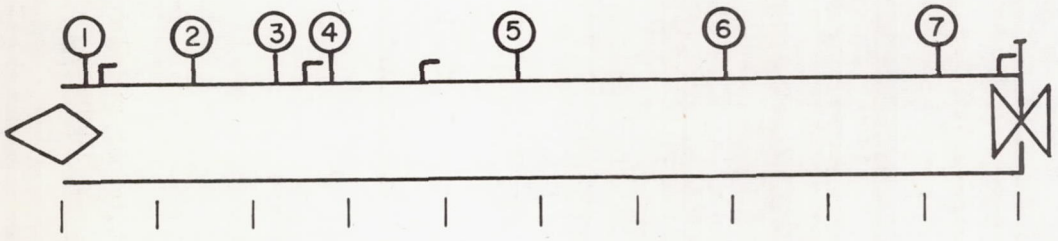

(c) Long diffuser; L = 390 inches.

Gate valve

(n) Location of pressure pickup, n (not necessarily same for various diffusers)

Location of 90° elbows

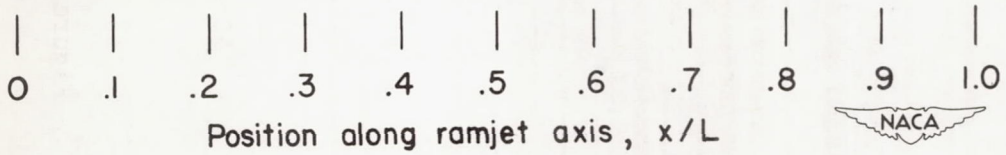

Figure 6.- Schematic diagram of ram-jet models tested showing: (1) relative length of central body to overall length, and (2) locations of pressure pick-ups and elbows.

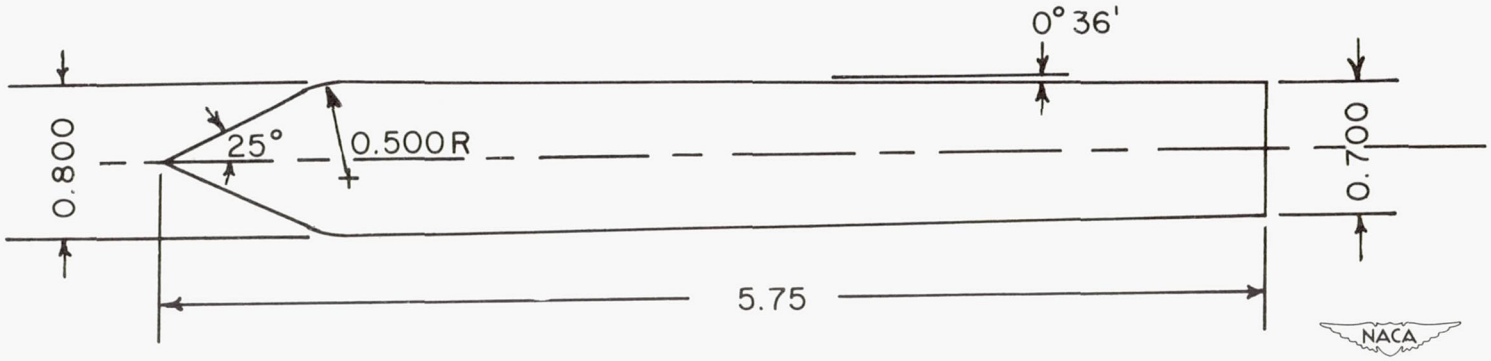

Figure 7.- Central body of configuration I. (Dimensions are in inches).

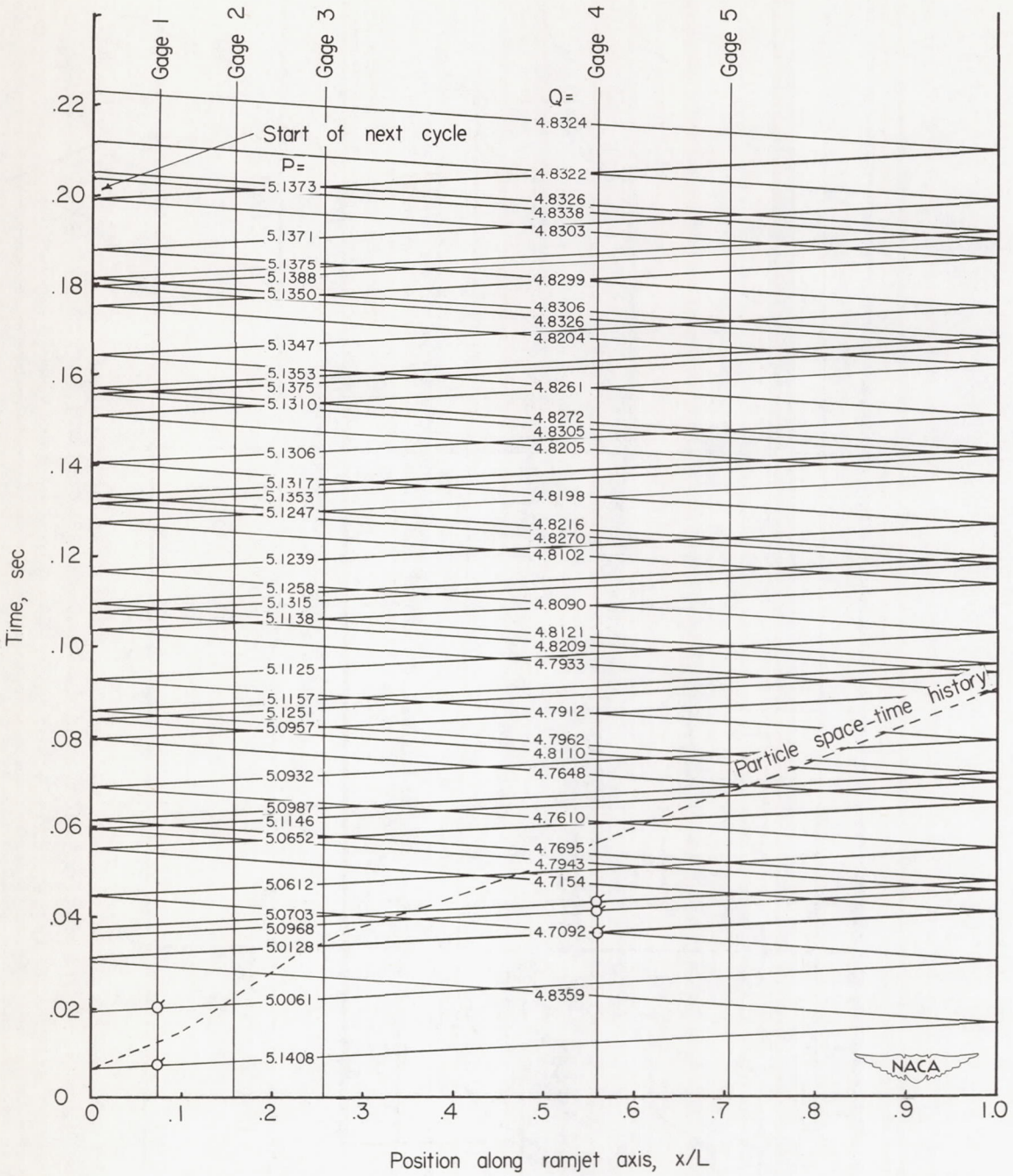

Figure 8.- Wave diagram for configuration I. $\theta_l = 44^\circ$; L = 156 inches. Flagged symbols denote points computed from experimental pressure record.

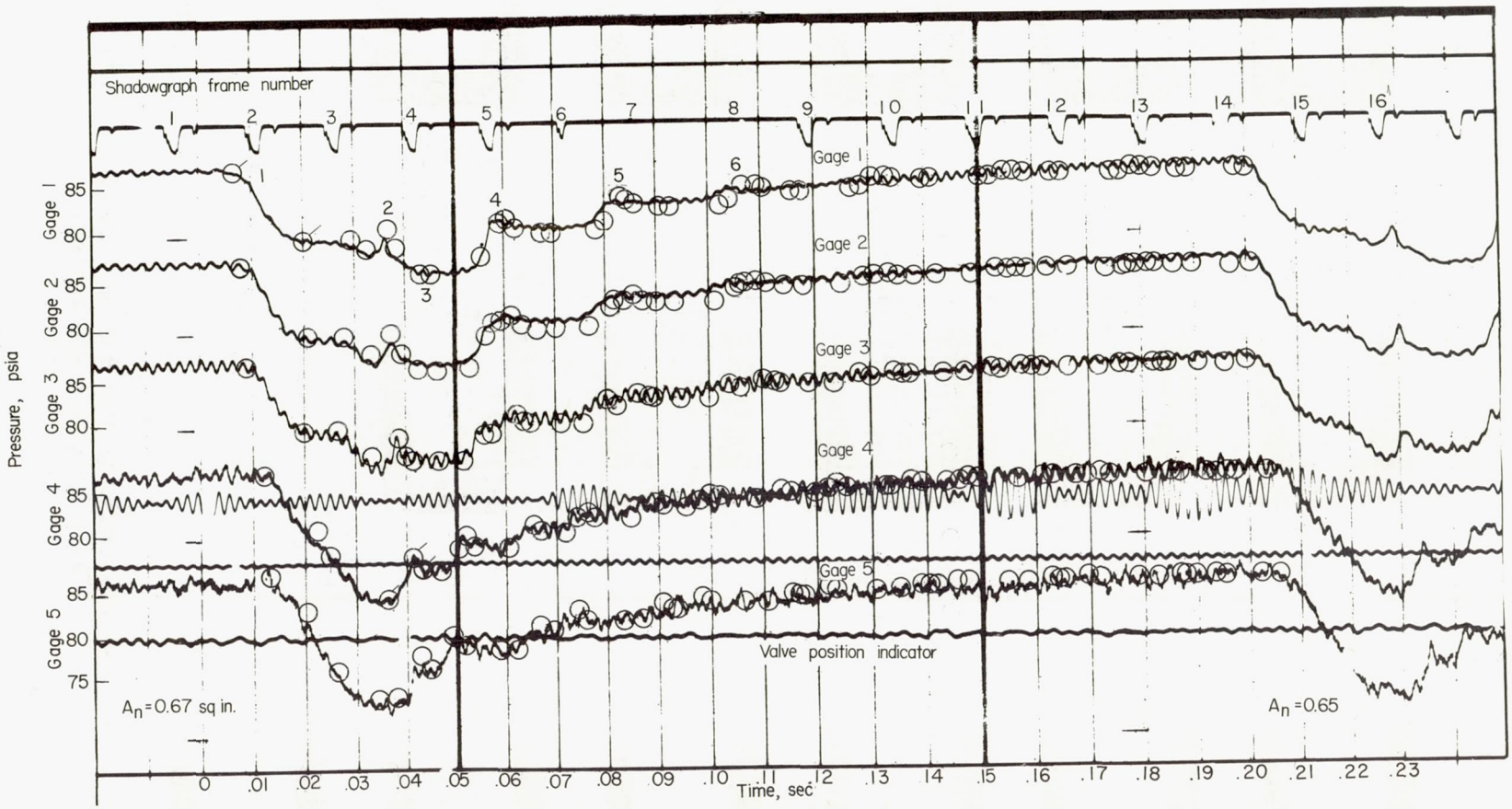

Figure 9.- Theoretical and experimental pressure-time curves for configuration I. $\theta_l = 44^\circ$; L = 156 inches. Flagged symbols denote experimental points on which theoretical computations are based.

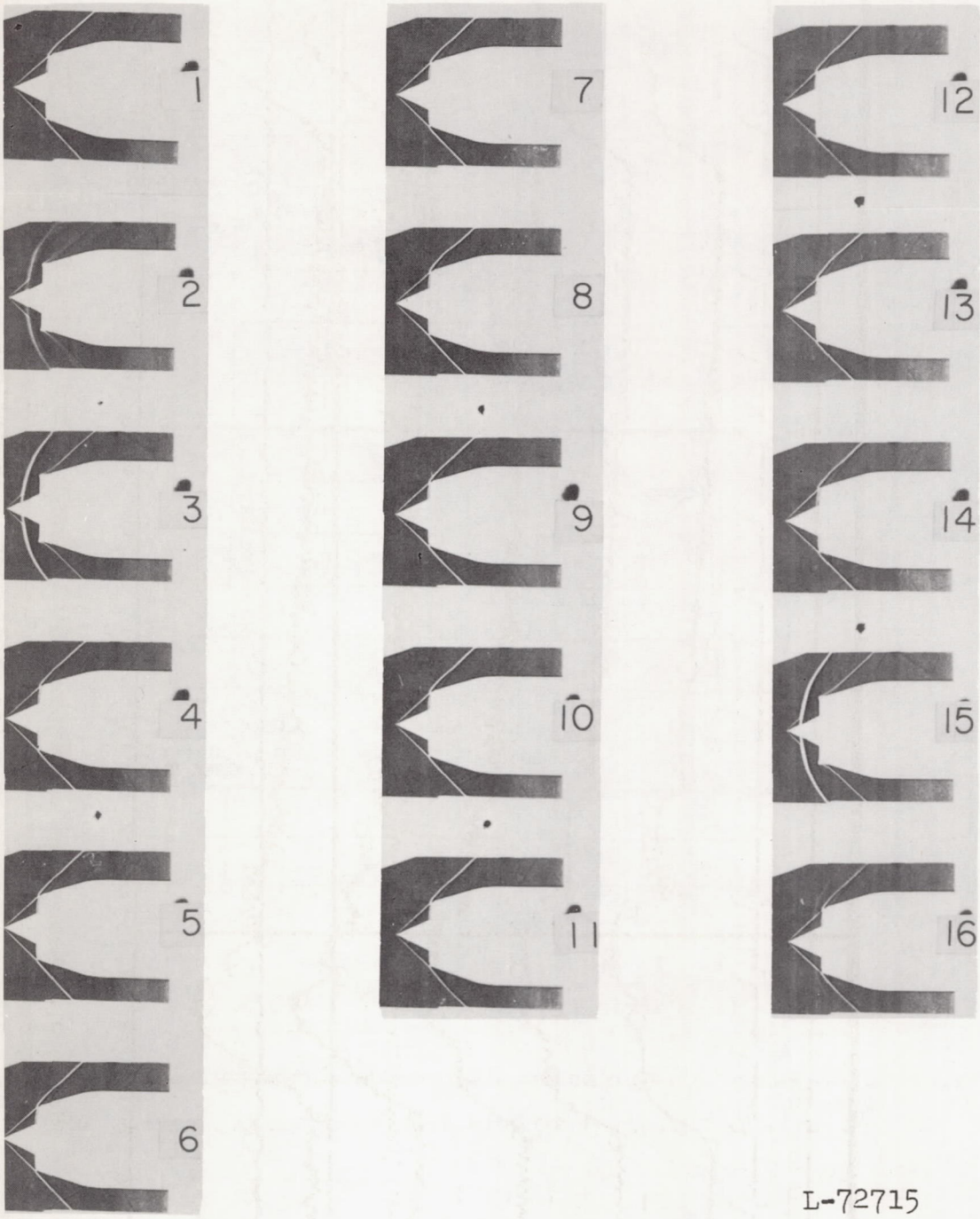

Figure 10.- Low-speed shadowgraphs during buzz of configuration I. $\theta_l = 44^\circ$; L = 156 inches.

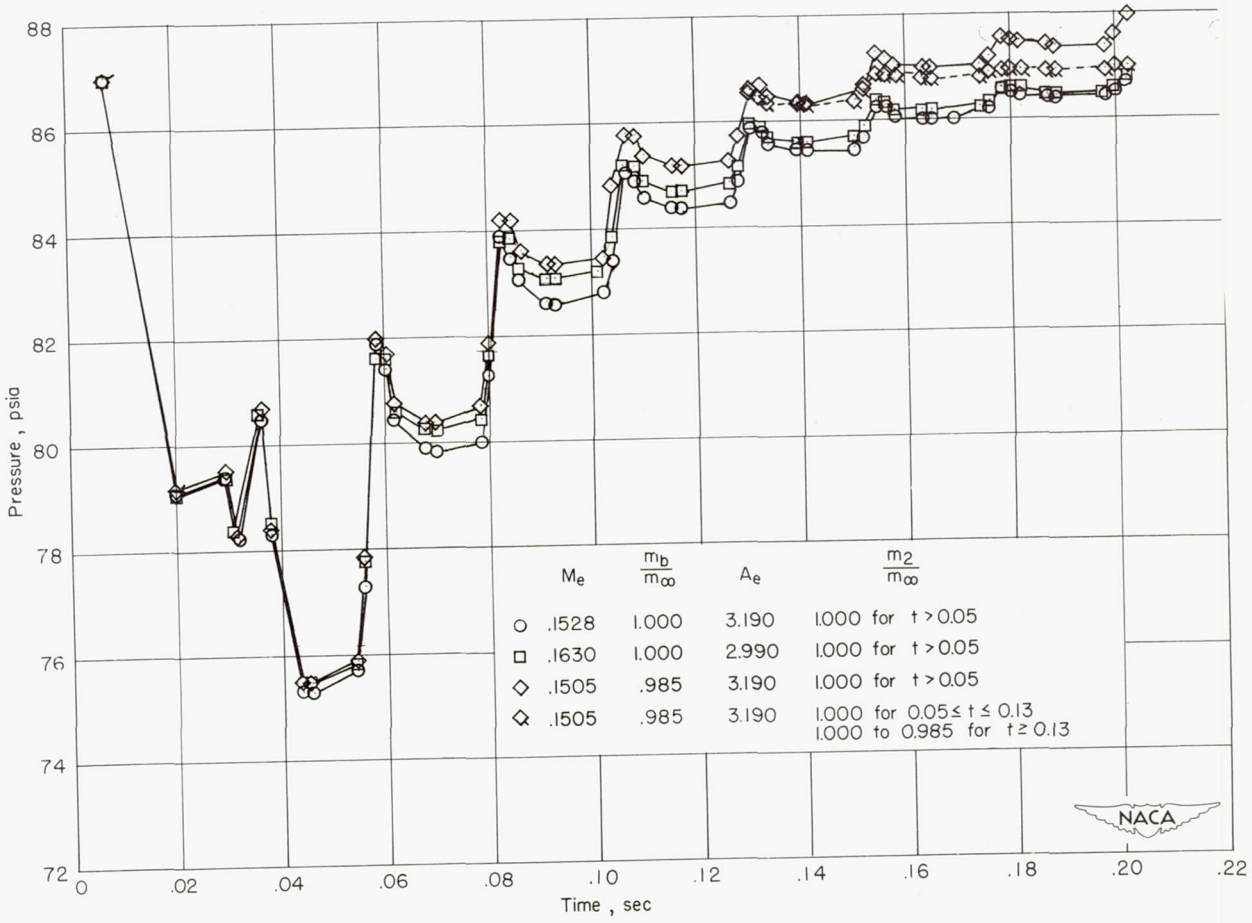

(a) Curves for gage 1 at $\frac{x}{L} = 0.074$.

Figure 11.- Theoretical pressure-time curves showing effect of variation in $\frac{m_b}{m_\infty}$ and A_e. Flagged symbols denote common pressures taken from experimental record.

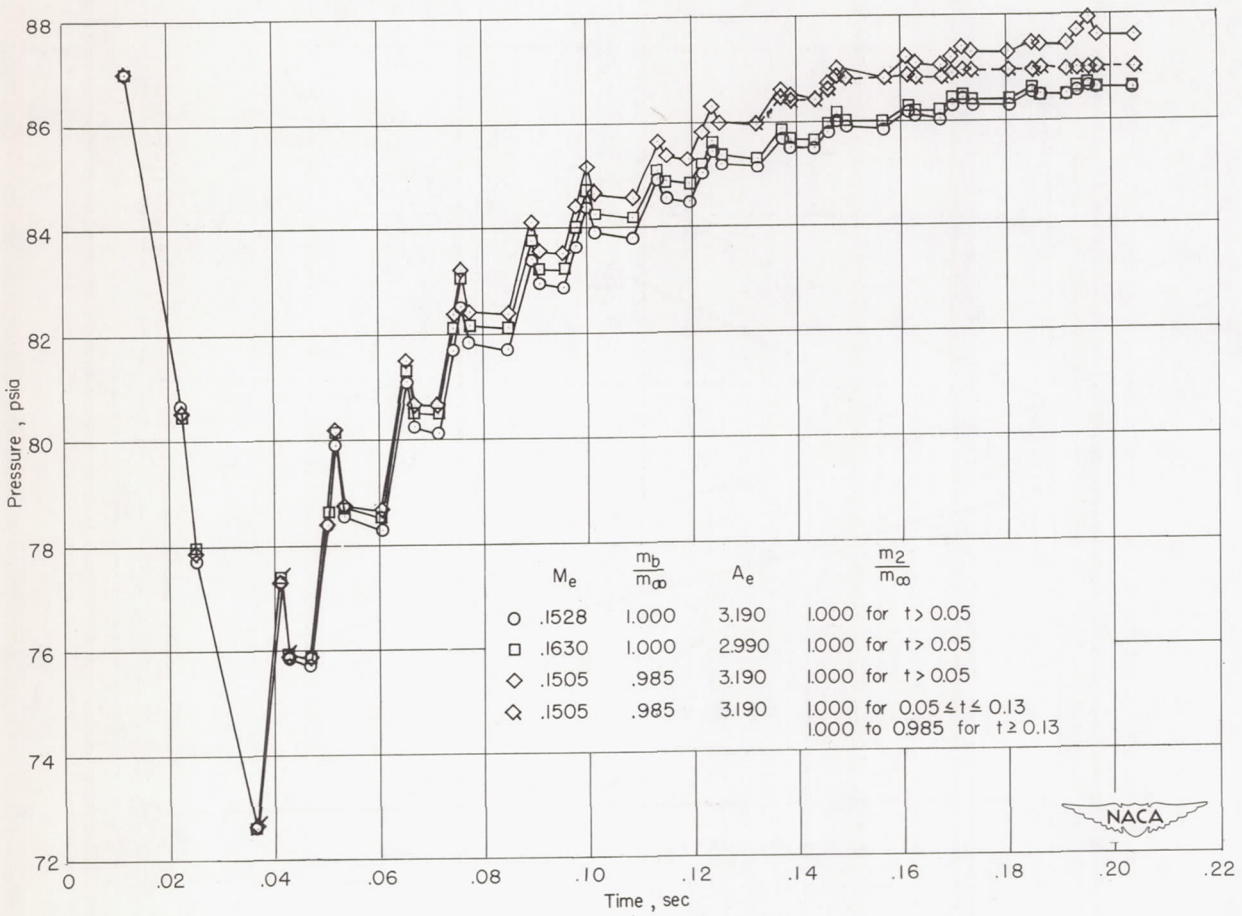

(b) Curves for gage 4 at $\frac{x}{L} = 0.558$.

Figure 11.- Concluded.

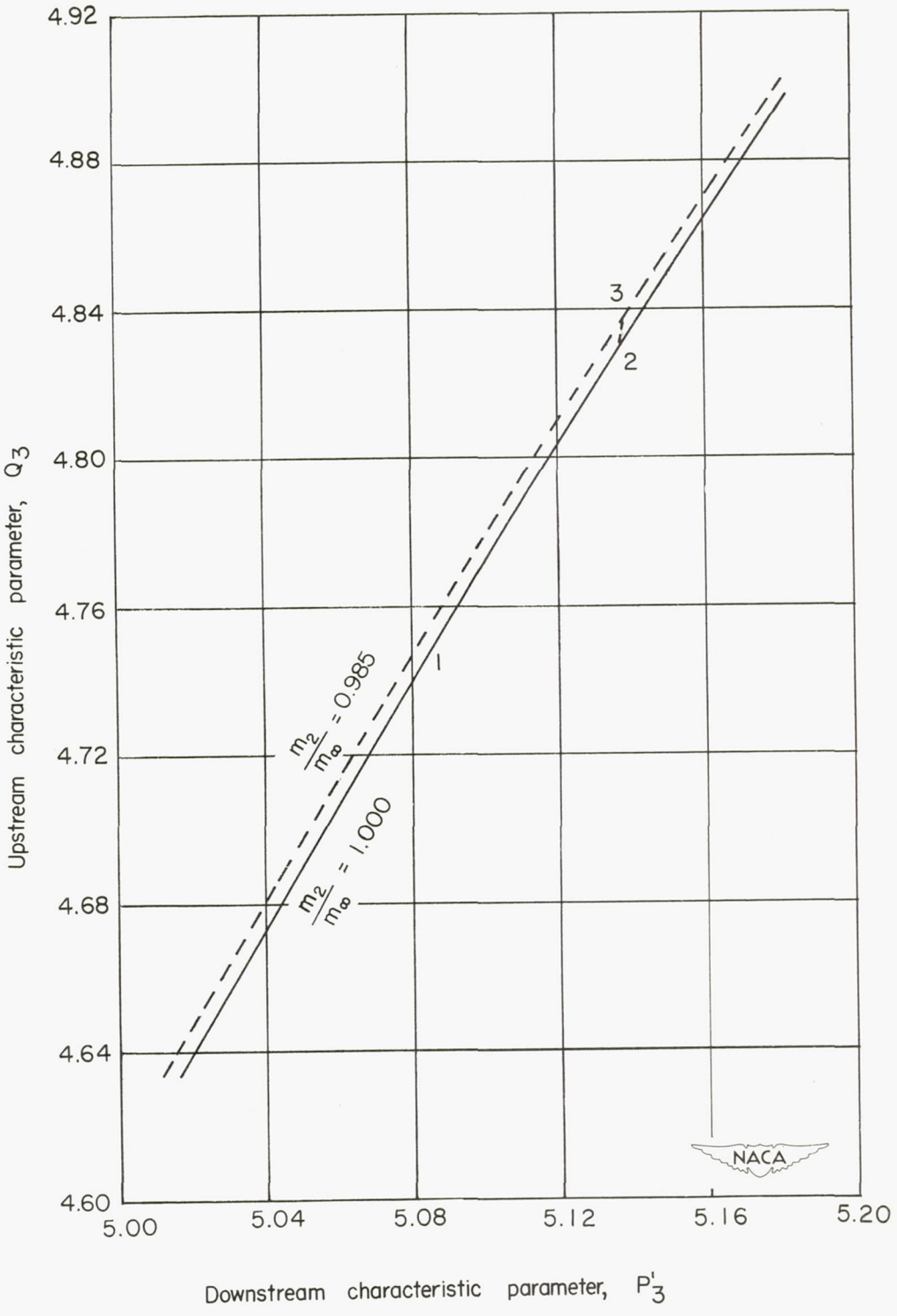

Figure 12.- Curves for determination of parameters reflected from inlet. Effective entropy $\frac{S_e}{R} = 0.1334$.

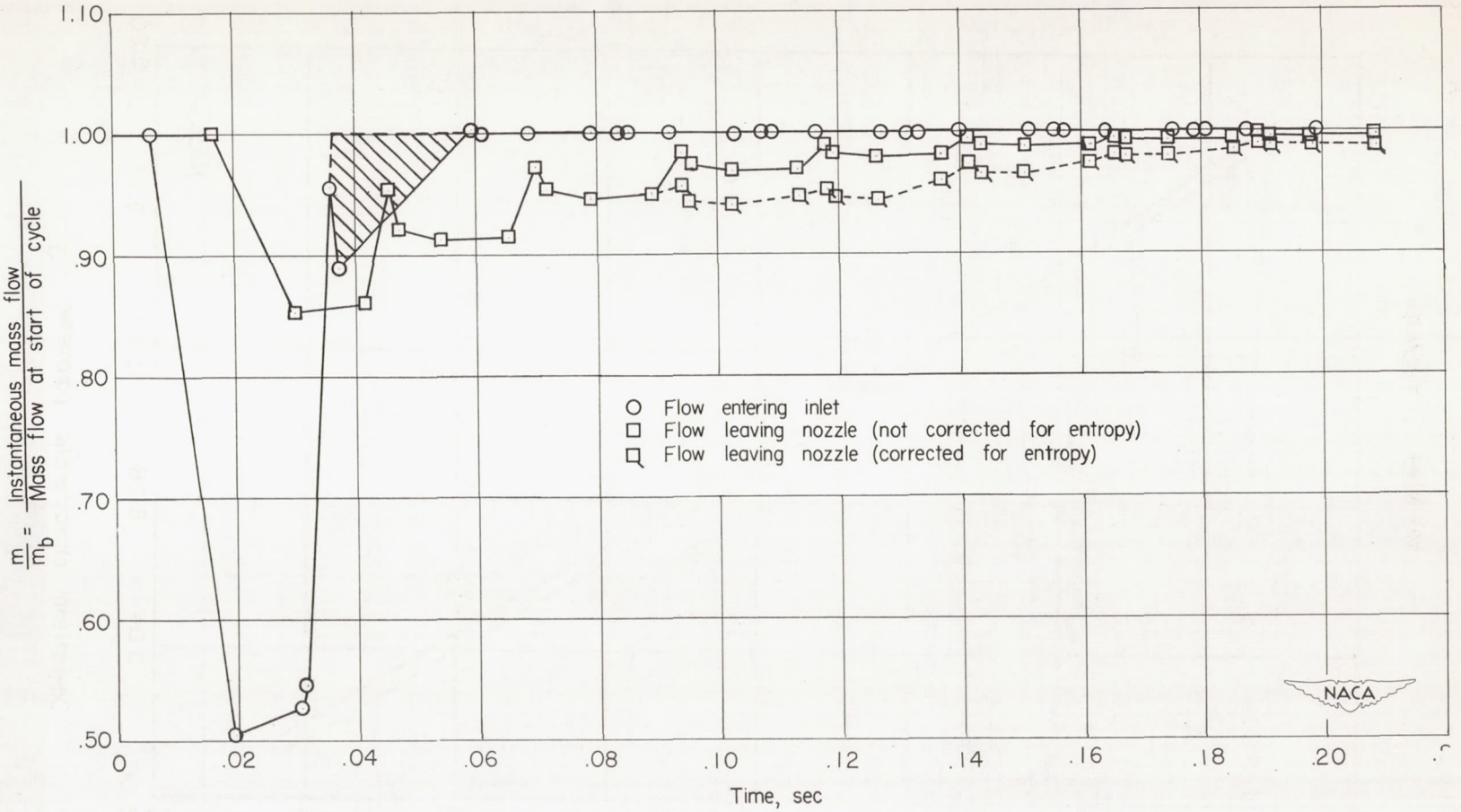

Figure 13.- Curves of instantaneous mass flow through inlet cowling and exit nozzle for configuration I. $\theta_l = 44^\circ$; L = 156 inches; $\frac{m_b}{m_\infty}$ is assumed to be equal to 1.000.

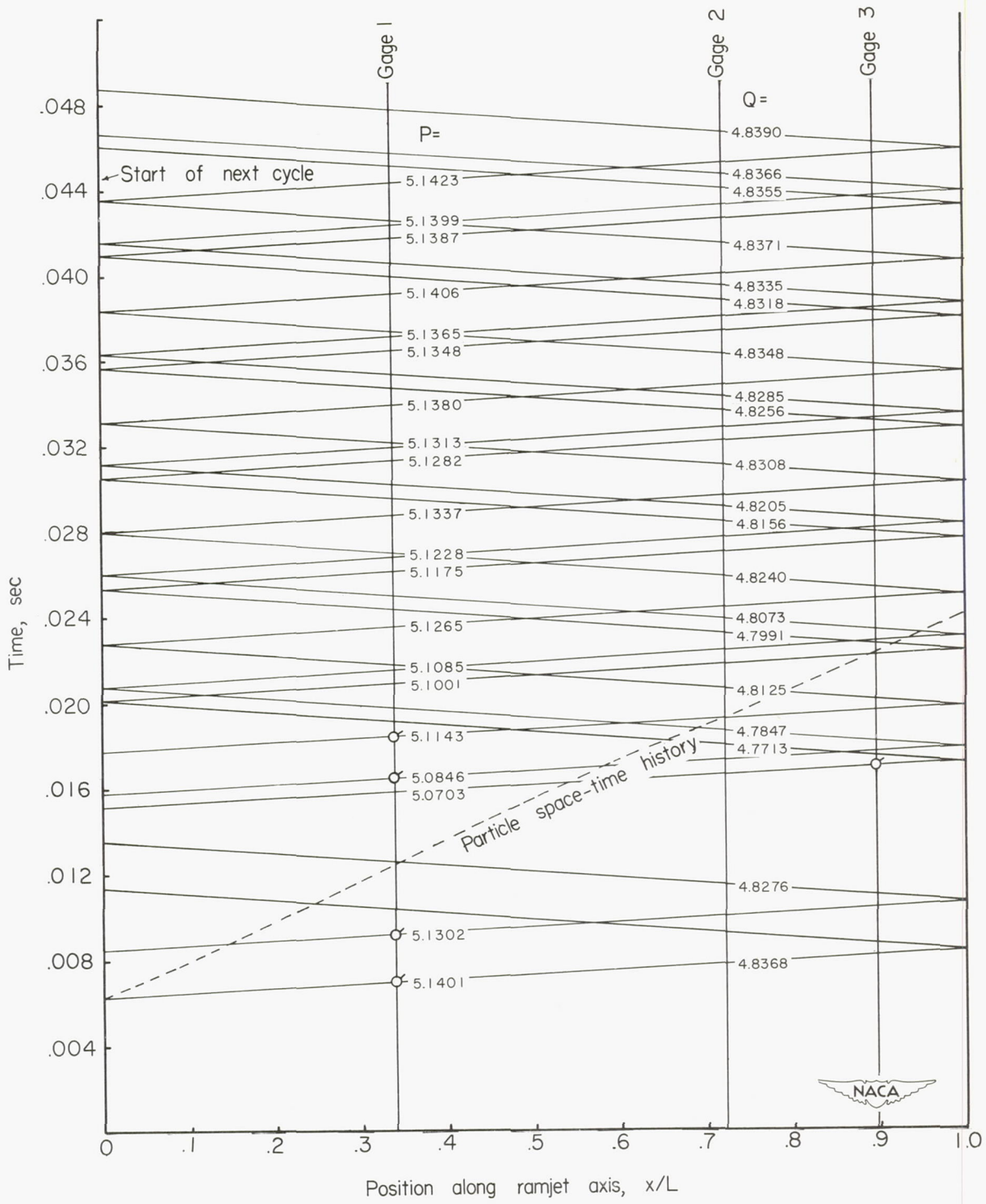

Figure 14.- Wave diagram for configuration I. $\theta_l = 44^\circ$; L = 34 inches. Flagged symbols denote points computed from experimental pressure record.

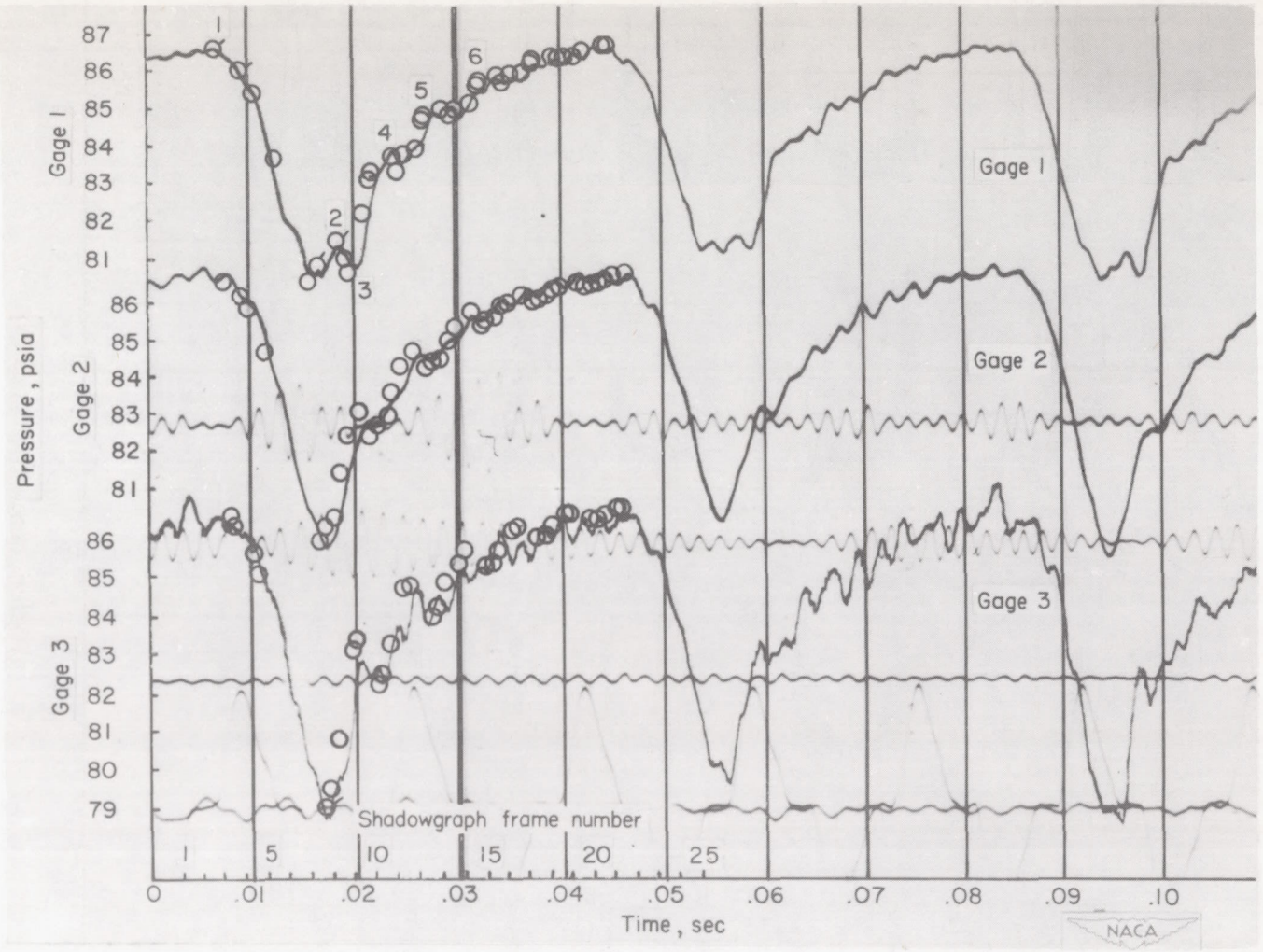

Figure 15.- Theoretical and experimental pressure-time curves for configuration I. $\theta_l = 44^\circ$; L = 34 inches. Flagged symbols denote experimental points on which theoretical computations are based.

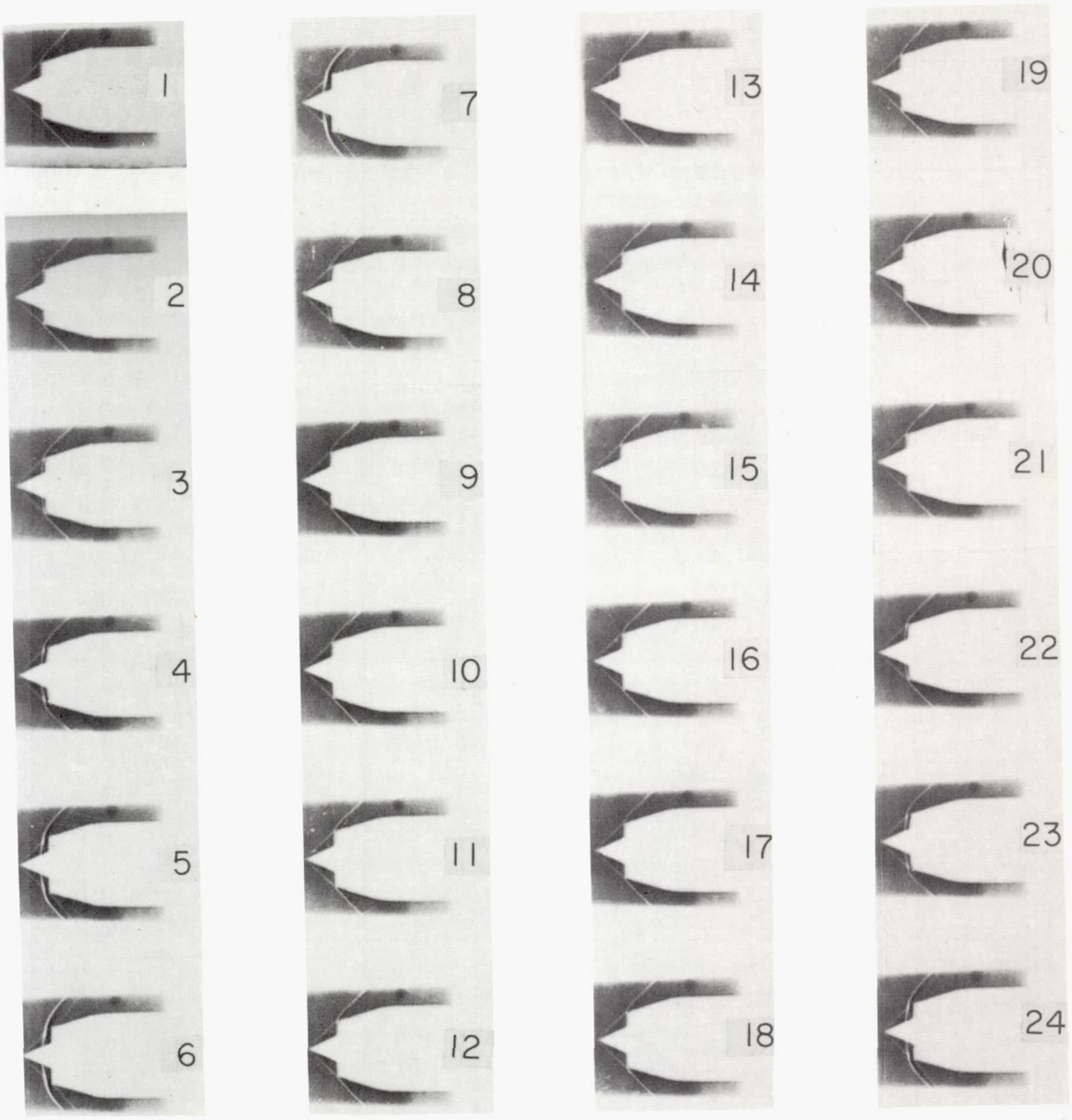

Figure 16.- High-speed shadowgraphs during buzz of configuration I. $\theta_l = 44^\circ$; L = 34 inches.

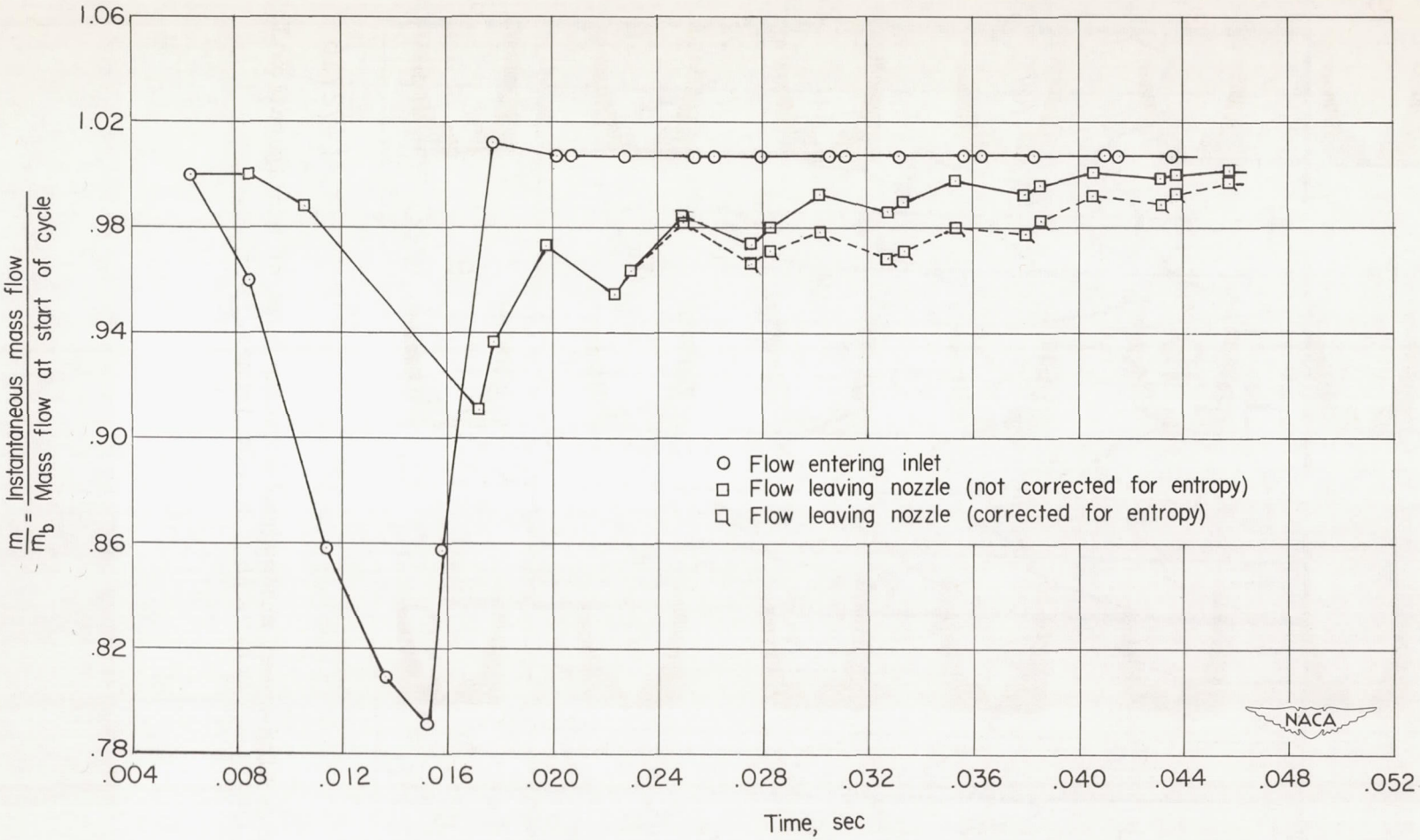

Figure 17.- Curves of instantaneous mass flow through inlet cowling and exit nozzle for configuration I. $\theta_l = 44^\circ$; L = 34 inches; $\frac{m_b}{m_\infty}$ is assumed to be equal to 0.993.

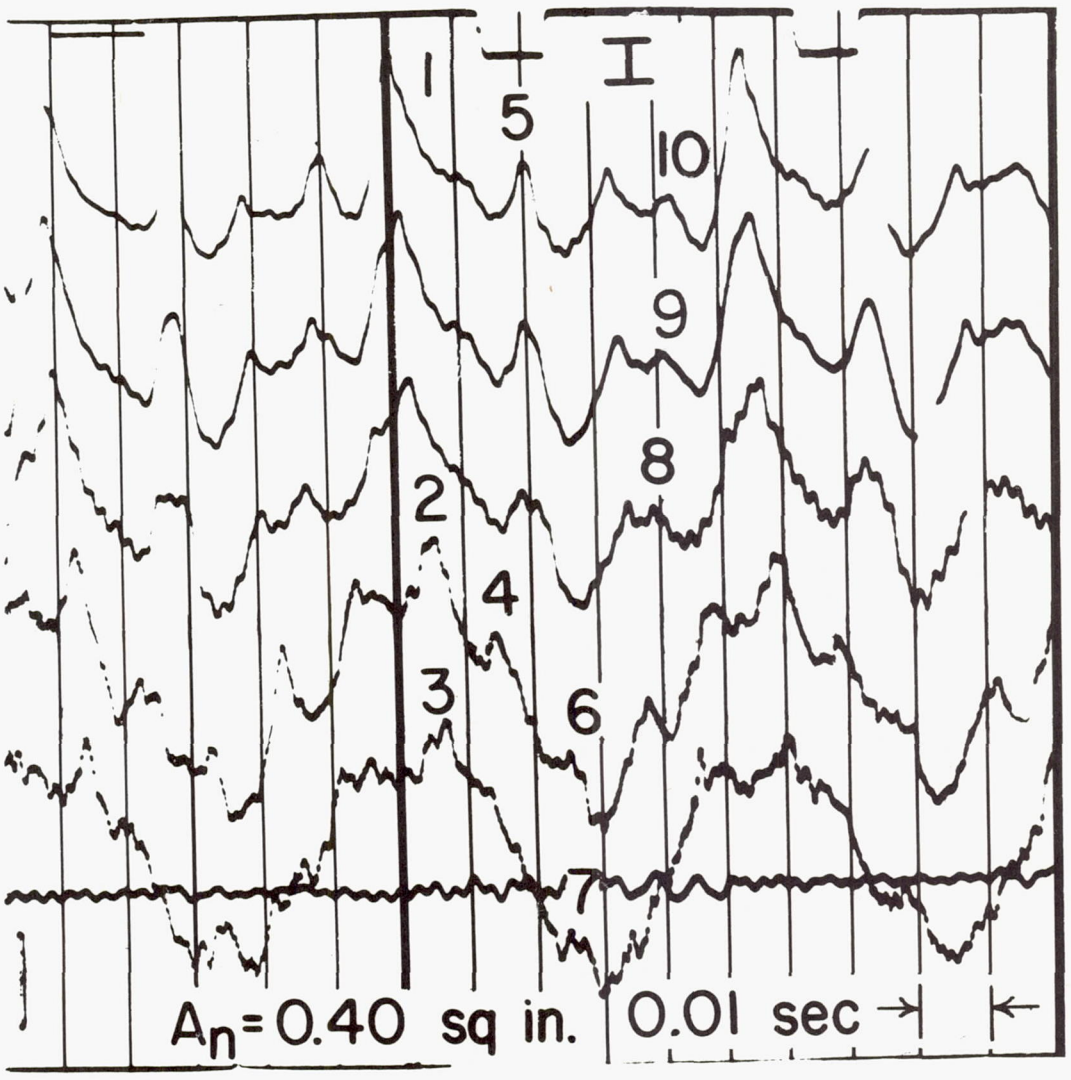

(a) Enlargement of region I.

Figure 18.- Pressure record obtained as exit throttle is rapidly opened for configuration I. $\theta_l = 44^\circ$; L = 156 inches.

(b) Complete record.

Figure 18.- Concluded.

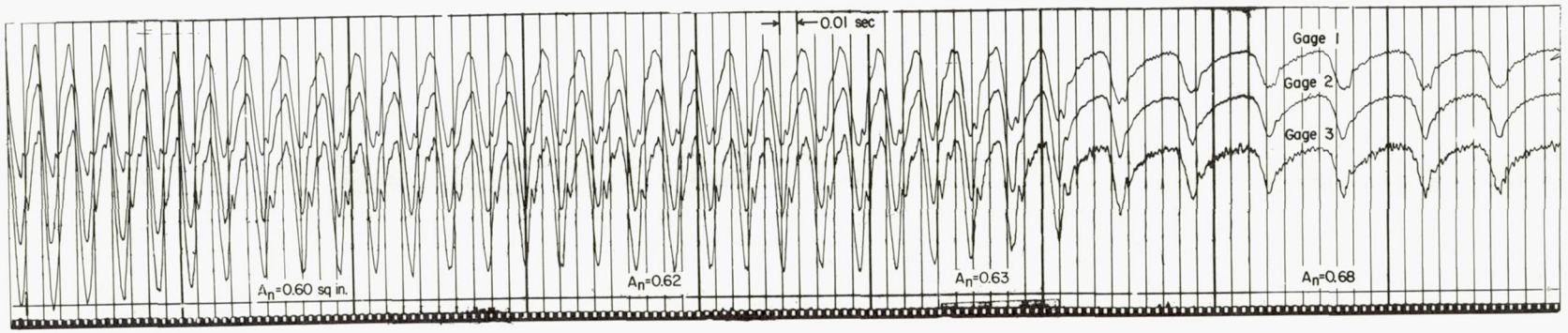

Figure 19.- Pressure record obtained as exit throttle is rapidly opened for configuration I. $\theta_l = 44^\circ$; L = 34 inches.

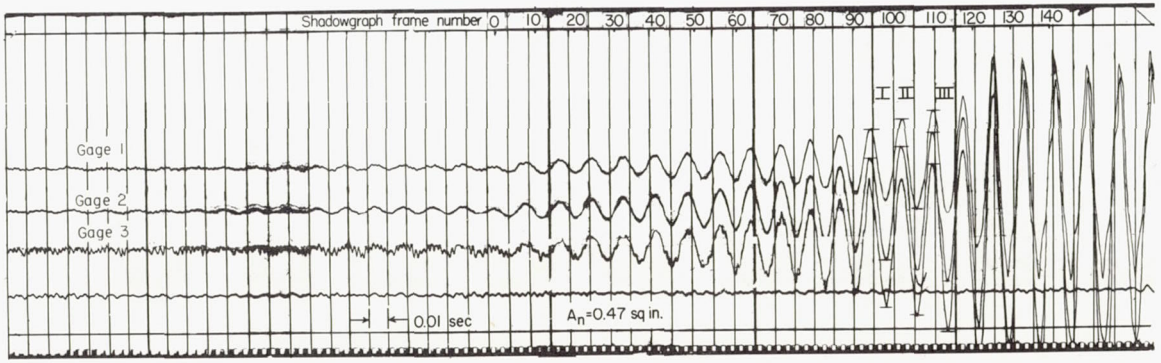

Figure 20.- Pressure record showing unstable oscillation as buzzing begins for configuration II. $\theta_l = 43^\circ\ 10'$; L = 34 inches.

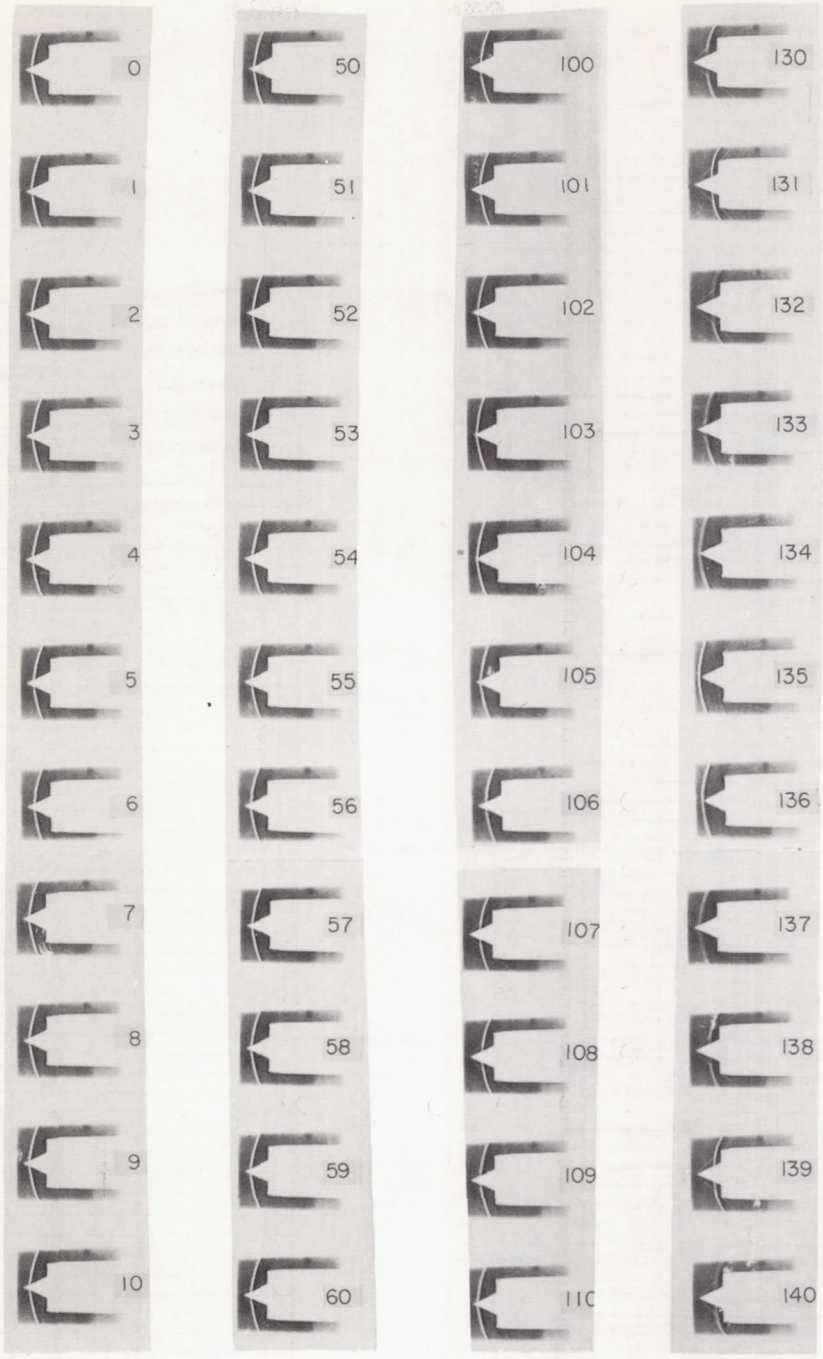

NACA

L-72717

Figure 21.- High-speed shadowgraphs during buzz of configuration II. $\theta_l = 43^\circ\ 10'$; L = 34 inches.

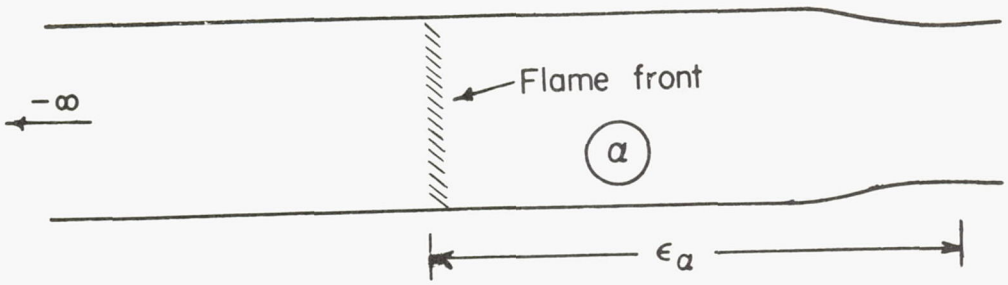

(a) Discontinuous heat addition in semi-infinite pipe.

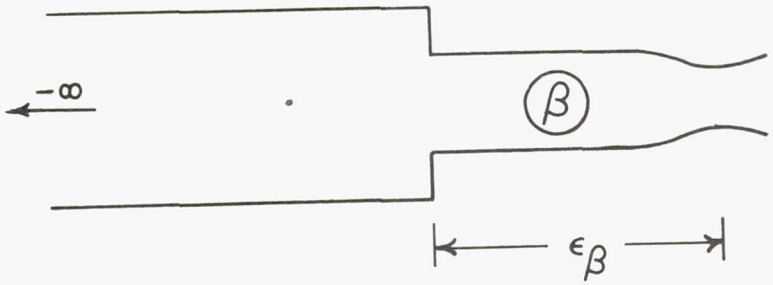

(b) Discontinuous area change in semi-infinite pipe.

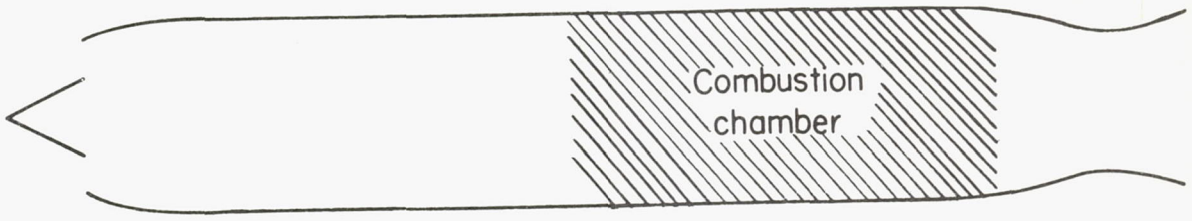

(c) Ram jet with finite combustion-chamber length.

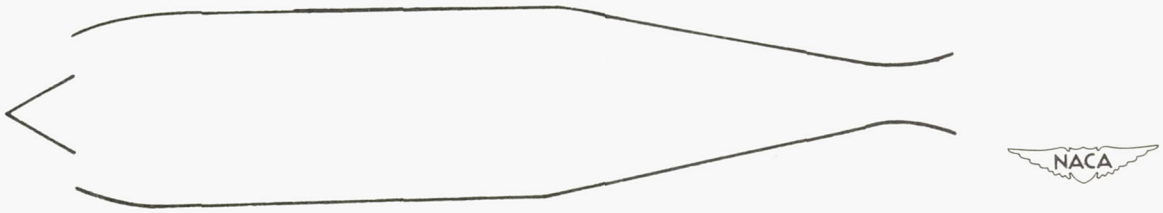

(d) Ram jet with gradual contraction of rear section.

Figure 22.- Configuration pairs for possible simulation of heat additions.

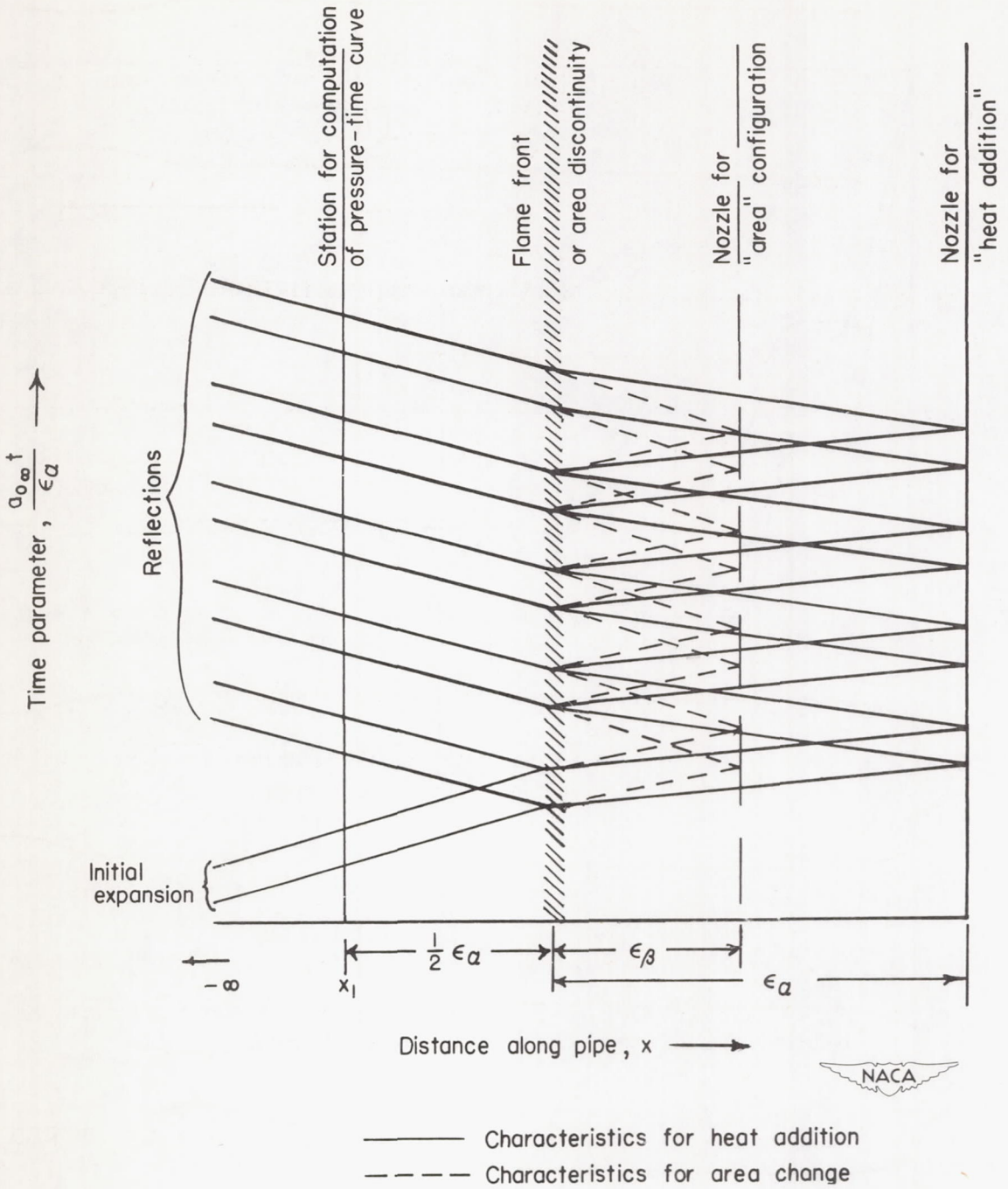

Figure 23.- Simplified wave diagram for heat addition and corresponding area contraction in semi-infinite pipe.

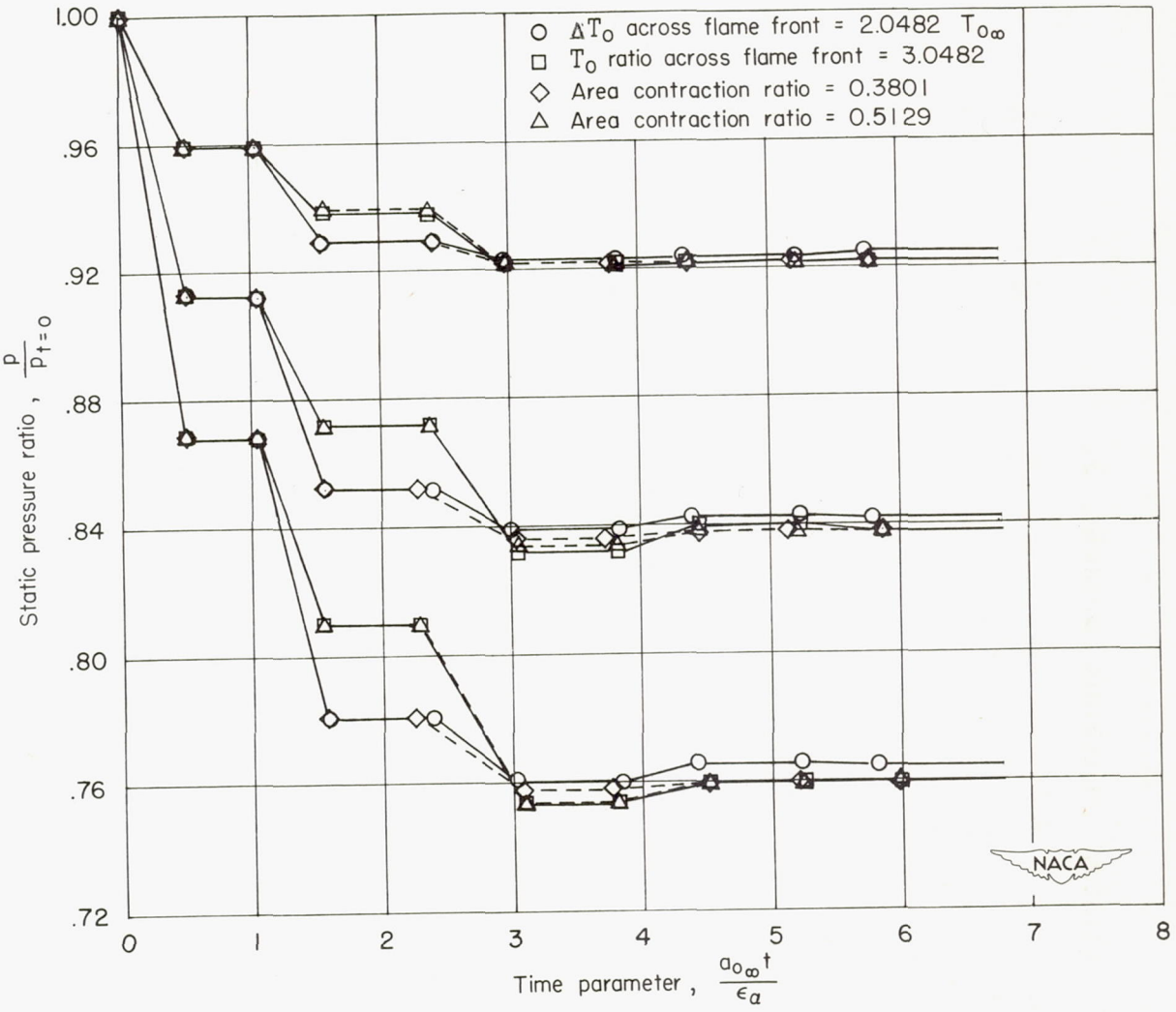

Figure 24.- Comparison of pressure-time curves for discontinuous heat addition and area contraction in semi-infinite pipe.

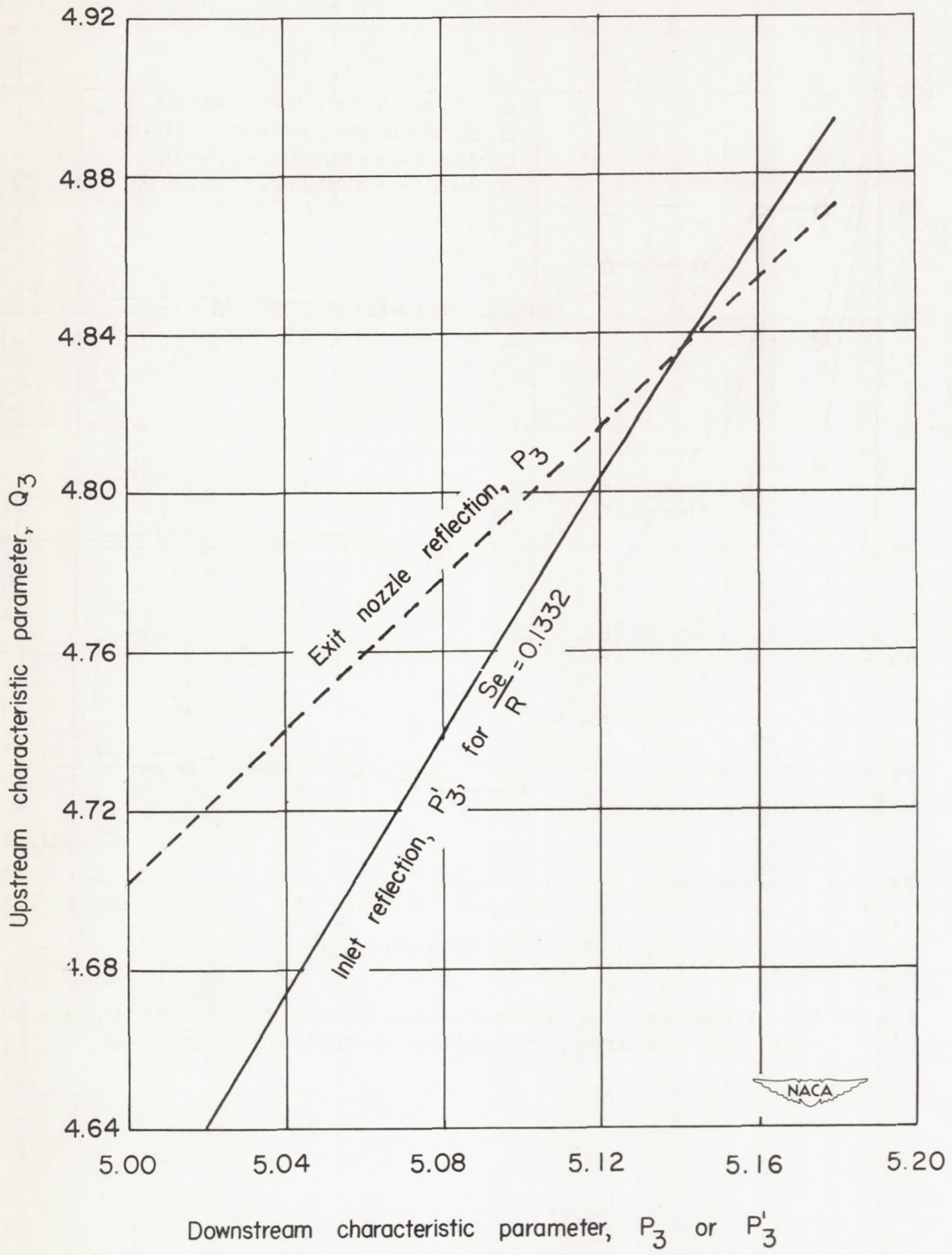

Figure 25.- Curves for determination of parameters reflected from cowling inlet and nozzle for configuration I. $\theta_l = 44^\circ$; L = 156 inches.

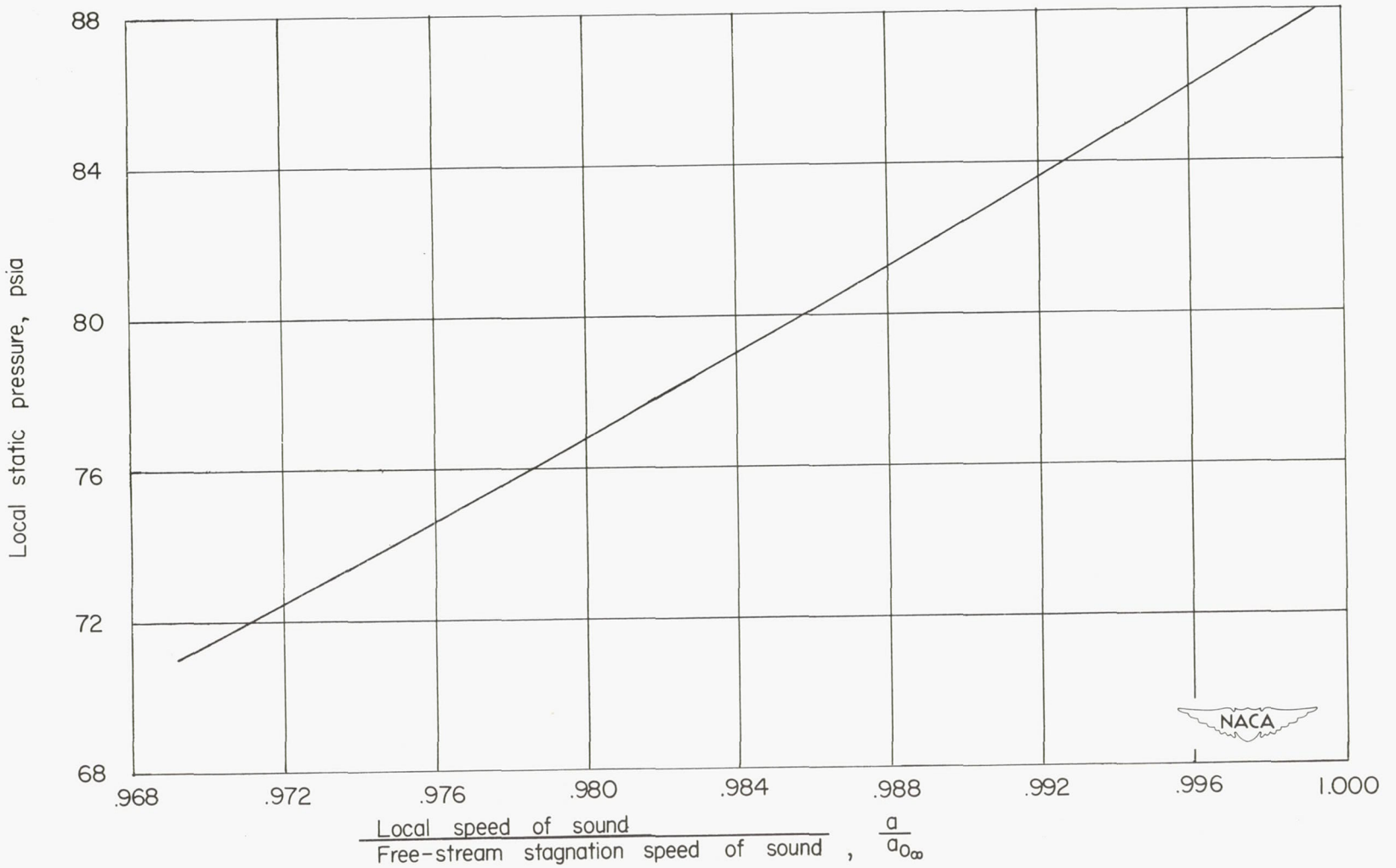

Figure 26.- Curve of local static pressure and local sonic speed for configuration I. $\theta_l = 44^\circ$; L = 156 inches.